AD-A116 298 DAVID W TAYLOR NAVAL SHIP RESEARCH AND DEVELOPMENT CE--ETC F/G 20/4
TRANSONIC WIND TUNNEL TEST OF A 16-PERCENT-THICK CIRCULATION CO--ETC(U)
APR 82 J B WILKERSON, P S MONTANA

UNCLASSIFIED DTNSRDC/ASED-82/03 NL

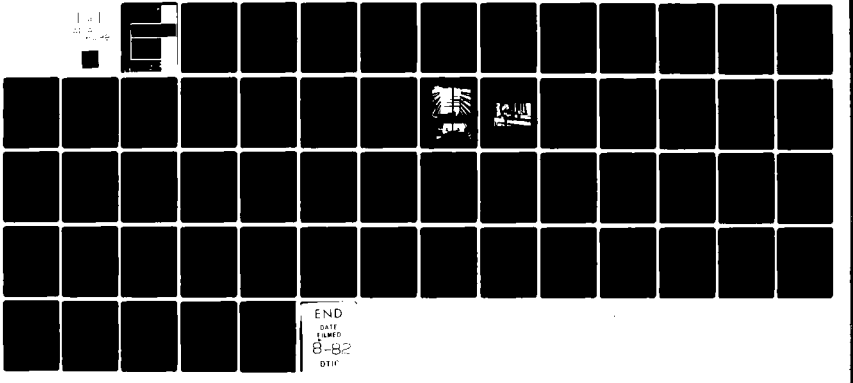

END
DATE FILMED
8-82
DTIC

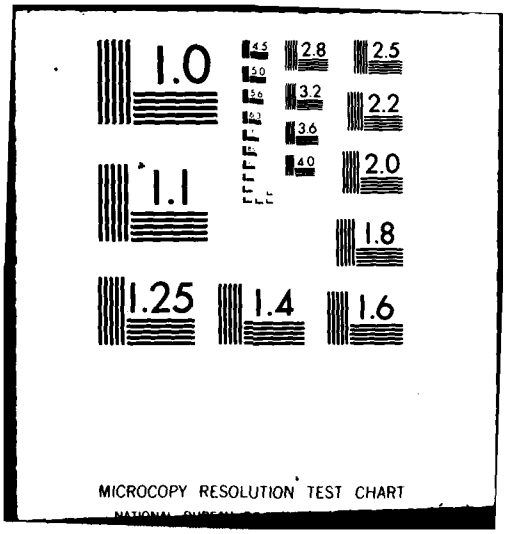
1.0
1.1
1.25
1.4
1.6
1.8
2.0
2.2
2.5
2.8
3.2
3.6
4.0
4.5
5.0
5.6
6.3
7.1
MICROCOPY RESOLUTION TEST CHART

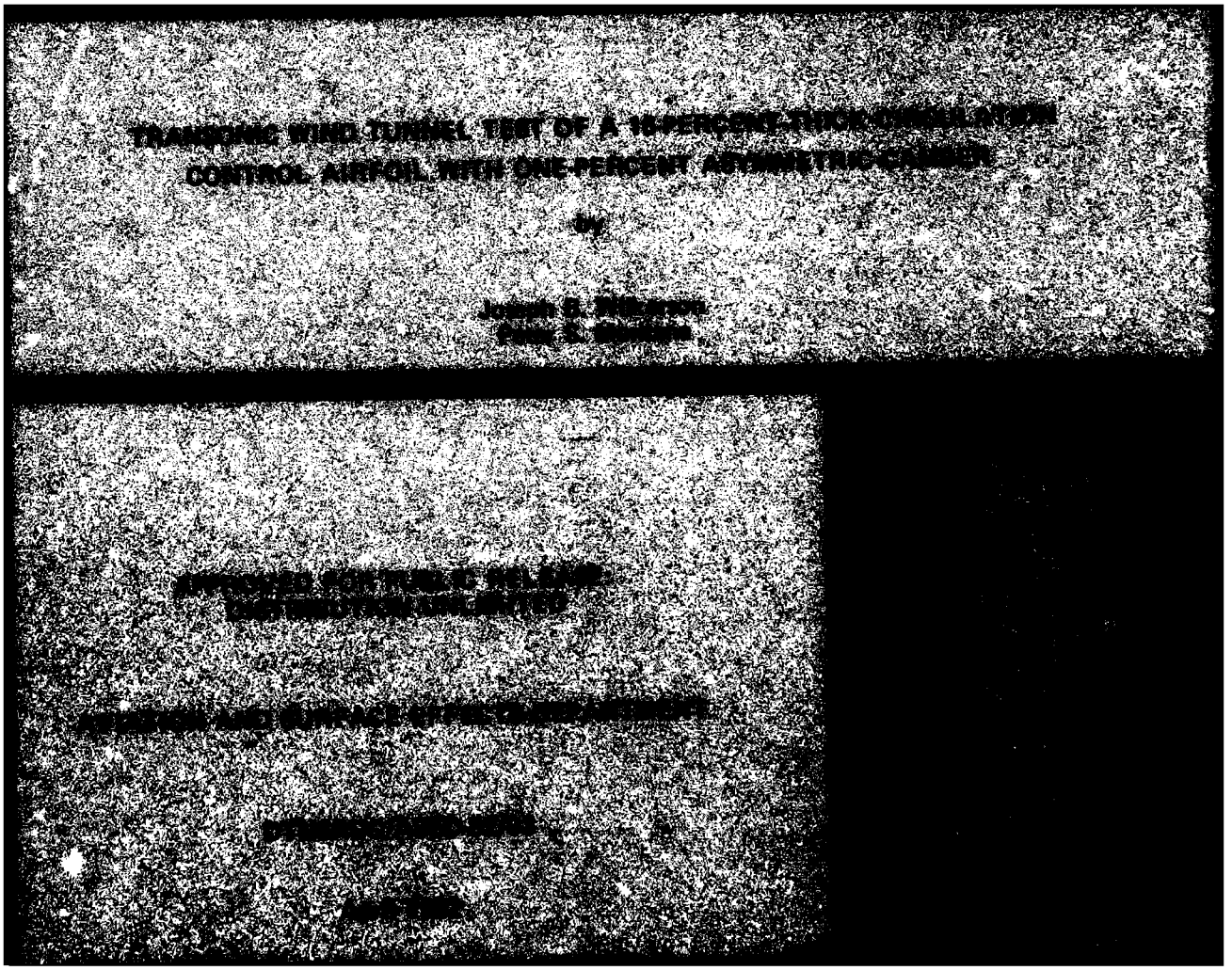

UNCLASSIFIED

SECURITY CLASSIFICATION OF THIS PAGE *(When Data Entered)*

REPORT DOCUMENTATION PAGE		READ INSTRUCTIONS BEFORE COMPLETING FORM
1. REPORT NUMBER DTNSRDC/ASED-82/03	2. GOVT ACCESSION NO. AD-A116 298	3. RECIPIENT'S CATALOG NUMBER
4. TITLE *(and Subtitle)* TRANSONIC WIND TUNNEL TEST OF A 16-PERCENT-THICK CIRCULATION CONTROL AIRFOIL WITH ONE-PERCENT ASYMMETRIC CAMBER		5. TYPE OF REPORT & PERIOD COVERED Final Report 6. PERFORMING ORG. REPORT NUMBER
7. AUTHOR*(s)* Joseph B. Wilkerson and Peter S. Montana		8. CONTRACT OR GRANT NUMBER*(s)*
9. PERFORMING ORGANIZATION NAME AND ADDRESS David Taylor Naval Ship R&D Center Aviation and Surface Effects Department Bethesda, Maryland 20084		10. PROGRAM ELEMENT, PROJECT, TASK AREA & WORK UNIT NUMBERS Program Element 63203N Task Area W0578001 Work Unit 1619-200
11. CONTROLLING OFFICE NAME AND ADDRESS Naval Air Systems Command AIR-320D Washington, D.C. 20361		12. REPORT DATE April 1982 13. NUMBER OF PAGES 61
14. MONITORING AGENCY NAME & ADDRESS*(if different from Controlling Office)*		15. SECURITY CLASS. *(of this report)* UNCLASSIFIED 15a. DECLASSIFICATION/DOWNGRADING SCHEDULE

16. DISTRIBUTION STATEMENT *(of this Report)*

APPROVED FOR PUBLIC RELEASE: DISTRIBUTION UNLIMITED

17. DISTRIBUTION STATEMENT *(of the abstract entered in Block 20, if different from Report)*

18. SUPPLEMENTARY NOTES

19. KEY WORDS *(Continue on reverse side if necessary and identify by block number)*

Helicopters
Airfoils
Circulation Control

20. ABSTRACT *(Continue on reverse side if necessary and identify by block number)*

A two-dimensional circulation control (CC) airfoil model was tested in the 7- by 10-foot transonic wind tunnel at the David W. Taylor Naval Ship R&D Center. Test conditions covered a range of free-stream Mach numbers (0.3 to 0.8), angles of attack (-10 to +6 deg), and blown jet pressure ratios (0 to 3.0). These data provided the first information on the influence of angle of attack on CC airfoil drag and lift augmentation at transonic speeds.

(Continued on reverse side)

DD FORM 1 JAN 73 1473 EDITION OF 1 NOV 65 IS OBSOLETE
S/N 0102-LF-014-6601

UNCLASSIFIED

SECURITY CLASSIFICATION OF THIS PAGE *(When Data Entered)*

(Block 20 continued)

The tested CC airfoil NCCR 1610-8054S was quasi-elliptical in shape, having a 16-percent thickness to chord ratio, with 1-percent maximum camber occuring at 70-percent chord. The program objectives were to achieve improved performance at transonic speeds while maintaining the characteristically high-lift augmentation at low subsonic operation. These objectives required nonsymmetrical thickness and camber distributions for the airfoil. Performance goals were qualitatively substantiated by the transonic test data. At 2-deg angle of attack, a maximum lift coefficient of 2.1 was obtained at $M_\infty \approx 0.3$; while for $M_\infty = 0.6$ at the same angle, the maximum lift coefficient was 0.76. As a high-lift device the airfoil was very effective at and below $M_\infty = 0.4$. As a means of direct lift control the airfoil remained effective up through $M_\infty = 0.7$.

TABLE OF CONTENTS

LIST OF FIGURES

NOTATION

a_j	Sonic velocity in the jet, ft/sec (m/s)
C_d	Sectional profile drag coefficient from momentum loss in wake, corrected for additional mass efflux of the jet
$C_{d_{rake}}$	Sectional profile drag coefficient as measured by rake, uncorrected
C_ℓ	Sectional lift coefficient
$C_{\ell_{max}}$	Maximum sectional lift coefficient obtainable within test C_μ limitations
C_{ℓ_o}	Unblown Lift Coefficient
$C_{m_{50}}$	Pitching moment coefficient about the half-chord
C_p	Pressure coefficient, $(P_\ell - P_\infty)/q_\infty$
C_p^*	C_p for local sonic flow
C_μ	Momentum coefficient, $\dot{m}V_j/(q_\infty S)$
c	Chord length, ft (m)
h	Slot height, in. (cm)
ℓ	Sectional lift, lb (kg)
M_{crit}	Critical Mach number
M_j	Mach number in the jet
M_∞	Free-stream Mach number
$\dot{m}$	Mass efflux, slugs/sec
P_ℓ	Local static pressure on the model, lb/ft^2 (N/m^2)
P_t	Duct (plenum) total pressure, lb/ft^2 (N/m^2)
P_{t_∞}	Free-stream total pressure, lb/ft^2 (N/m^2)
P_∞	Free-stream static pressure, lb/ft^2 (N/m^2)
q_∞	Free-stream dynamic pressure, lb/ft^2 (N/m^2)
R	Universal gas constant
R_e	Reynolds number based on chord
S	Model planform area, ft^2 (m^2)

T_j	Jet static temperature, °R
T_t	Duct (plenum) total temperature, °R
t	Airfoil thickness, ft (m)
V_j	Jet velocity, ft/sec (m/s)
V_∞	Free-stream velocity, ft/sec (m/s)
x	Chordwise distance from leading edge, ft (m)
x_s	Chordwise distance of the slot from leading edge, ft (m)
x/c	Dimensionless chordwise position
α	Geometric angle of attack, deg
γ	Ratio of specific heats

ABSTRACT

A two-dimensional circulation control (CC) airfoil model was tested in the 7- by 10-foot transonic wind tunnel at the David W. Taylor Naval Ship R&D Center. Test conditions covered a range of free-stream Mach numbers (0.3 to 0.8), angles of attack (-10 to +6 deg), and blown jet pressure ratios (0 to 3.0). These data provided the first information on the influence of angle of attack on CC airfoil drag and lift augmentation at transonic speeds. The tested CC airfoil NCCR 1610-8054S was quasi-elliptical in shape, having a 16-percent thickness to chord ratio, with 1-percent maximum camber occuring at 70-percent chord. The program objectives were to achieve improved performance at transonic speeds while maintaining the characteristically high-lift augmentation at low subsonic operation. These objectives required nonsymmetrical thickness and camber distributions for the airfoil. Performance goals were qualitatively substantiated by the transonic test data. At 2-deg angle of attack, a maximum lift coefficient of 2.1 was obtained at $M_\infty = 0.3$; while for $M_\infty = 0.6$ at the same angle, the maximum lift coefficient was 0.76. As a high-lift device the airfoil was very effective at and below $M_\infty = 0.4$. As a means of direct lift control the airfoil remained effective up through $M_\infty = 0.7$.

ADMINISTRATIVE INFORMATION

The work reported herein was funded under Naval Air Systems Command (AIR-320D) Program Element 63203N, Task Area WO578001, and David W. Taylor Naval Ship R&D Center (DTNSRDC) Work Unit 1-1619-200. This effort was part of an ongoing task to expand the data base for circulation control airfoil two-dimensional characteristics.

INTRODUCTION

The circulation control (CC) airfoil development program was initiated under the CC Rotor (CCR) Project in fiscal year 1976. The objectives of this ongoing task were to expand the two-dimensional data base for both subsonic and transonic data and to pursue the design and test evaluation of new CC airfoil contours for specific performance improvements. An overview of this work giving program background and design rationale for the airfoils tested was reported by Wilkerson.[1*] Subsonic wind tunnel tests, documented by Abramson,[2,3] have significantly extended

*A complete listing of references is given on page 11.

the CC airfoil data base. Performance characteristics of lift, drag, and pitching moment were established for several new, but related, airfoil geometries. Also, some effects of trailing edge geometry were explored, including a wide range of slot height-to-chord ratios.

The two most significant new profiles were designed analytically without restrictions as to thickness or camber distribution. The objective for each of the two designs was to maintain high levels of augmentation ($\Delta C_\ell / \Delta C_\mu$) at low subsonic speeds while increasing the critical Mach number values. Both designs achieved these goals analytically.[1] One of the two airfoil designs, designated NCCR 1610-8054S, was chosen for subsequent transonic wind tunnel evaluation, and the test results are reported herein.

The CC airfoil NCCR 1610-8054S was tested in the 7- by 10-Foot transonic wind tunnel at DTNSRDC. The test was conducted over a range of Mach numbers (0.3 to 0.8), angle of attack (-10 to +6 deg), and blown jet pressure ratios (0.0 to 3.0). This was the first transonic test providing data to evaluate the augmentation and drag divergence variation with angle of attack.

The airfoil profile (designed by E.O. Rogers*) is nominally a 16-percent-thick airfoil having a 1-percent camber line with maximum offset at the 70-percent chord location. The camber line was designed with zero slope at the leading edge. This feature minimizes lower surface leading edge suction peaks at negative angles of attack, which are operationally typical on CC rotor applications. Thickness distribution is that of a modified ellipse. The leading edge radius is reduced from a pure elliptical contour by using a power function redistribution of the ellipse coordinates, which also ensures continuity of surface derivatives. The trailing edge Coanda surface uses a spiral contour. The local surface radius-to-chord ratio negotiates from $r/c = 0.022$ just aft of the slot to a maximum value of $r/c = 0.040$ as it becomes tangent with the lower surface. Slot location is at $x_s/c = 0.980$, which is slightly further aft than on previous CC airfoil designs. Figure 1 shows the airfoil contour and camber line.

*Reported informally by Ernest O. Rogers, ("Design of a Circulation Control Airfoil for Application to Helicopter Rotors," DTNSRDC/TM-16-76/33, November 1975).

MODEL AND TEST APPARATUS

MODEL

The NCCR 1610-8054S airfoil shape was developed to meet the high-speed, high Reynolds number flow conditions encountered near the tip of a helicopter rotor. The airfoil model was constructed at full size for an 11,000-lb (5000-kg) helicopter to avoid the uncertainty of scale effects. Thus, the chord dimension of the airfoil was 18 in. (47.72 cm).

The model, designed by Clark,[4] was fabricated entirely of 7075-T6 aluminum. A single material was used for the airfoil model's four main pieces to minimize the possibility of model warpage due to temperature variation during the test. High strength aluminum was chosen because of its density, strength, and machinability. The resulting model was over 12 ft (3.66 m) long with about 10.1 ft (3.05 m) machined to the airfoil contour, Table 1.

The airfoil was composed of an upper section, a lower section, a trailing edge, and a knife edge; see Figure 2. The upper and lower sections form the leading edge and main structure of the airfoil. The knife edge and trailing edge were designed as separate components to allow for easy modifications of this area of the airfoil contour. (This critical area gives the airfoil its unique circulation control properties.) Air enters the airfoil through ducts at either end of the airfoil and exits the airfoil through the slot formed by the trailing edge and the knife edge. A design feature of the airfoil model was variable slot height. For this experiment, slot height was statically set at 0.030 in. (0.0762 cm).

In order to gather data, the airfoil model was pressure tapped. The primary pressure taps were located at the midspan. Additional pressure taps were placed at other spanwise locations to verify the two-dimensionality of the flow. Pressure tap locations are listed in Table 1.

TEST APPARATUS

The wind tunnel evaluation was carried out in the 7- by 10-foot transonic wind tunnel at DTNSRDC.[5] The facility is a closed-loop design capable of Mach numbers up to 1.17. It is possible to simulate a variety of atmospheric pressure conditions by running the tunnel evacuated, pressurized, or with settling chamber or test section vented. For this experiment the settling chamber was vented to the atmosphere. The net result of conducting the experiment with the settling chamber vented was that Reynolds number did not vary linearly with Mach number, as

would be expected for level flight conditions. In effect, altitude increased with Mach number. The actual Reynolds number range during the experiment was from 3.02×10^6 to 5.93×10^6 for Mach numbers from 0.3 to 0.8, rather than Reynolds numbers from 3.19×10^6 to 8.51×10^6 for constant altitude sea level flight.

The two-dimensional airfoil model was mounted horizontally in the wind tunnel as shown in Figure 3. The model was supported by a rotatable platform at each end and by two struts which were pinned through the lower surface of the airfoil. This support arrangement made it possible to remotely vary the angle of attack of the model.

Air for the trailing edge blowing was supplied to the airfoil through ducts attached (outside the test section) to either end of the model as shown in Figure 4. These ducts came from a common supply line located beneath the test section in the settling chamber. Control of the duct airflow was accomplished remotely using a pneumatically actuated valve.

During the experiment, data were taken for surface pressure, duct pressure and temperature, wake rake static and total pressures, and mass flow measurement. The airfoil surface pressures were recorded using two multi-ganged Scani-valves which were referenced to the wind tunnel free-stream static pressure. The surface pressure data were integrated in the data reduction process to calculate the lift force and pitching moment on the airfoil. Drag force was computed from pressure data obtained with the wake rake. The wake rake consisted of five total pressure probes and one static pressure probe mounted on a strut which vertically traversed the wake behind the model at the midspan station. Each probe was connected to a pressure transducer, and the wake data were recorded simultaneously with the surface pressure data.

Mass flow for the Coanda (trailing edge) blowing was computed from pressure and temperature data taken on standard venturi meters mounted in the supply lines to the airfoil duct. Coanda jet velocity was computed from pressure and temperature data measured at three locations within the blade duct.

DATA REDUCTION

Measured surface pressures were converted into local C_p values and then integrated to obtain airfoil lift and pitching moment coefficients about the half-chord point. Drag coefficients were obtained by integration of the wake rake measured pressures according to the method of Betz and Jones.[6] Final drag

coefficients include the added term $\dot{m}\, V_\infty/q_\infty S$ to account for the momentum increase from the Coanda jet.

The momentum coefficient was calculated from the measured model jet mass flow, and from the jet velocity V_j where

$$V_j = \sqrt{\gamma R T_t\, M_j^2 / \left(1 + \frac{\gamma+1}{2} M_j^2\right)}$$

and

$$M_j^2 = \frac{2}{\gamma-1}\left[\left(\frac{P_t}{P_\infty}\right)^{\frac{\gamma-1}{\gamma}} - 1\right]$$

These equations assume a pure isentropic expansion from model duct total pressure to free-stream static pressure. The above relations were applied for all pressure ratios, thus yielding jet Mach numbers greater than 1.0 for high pressure ratios.

Test section Mach number and dynamic pressure were calculated using the relations:

$$M_\infty^2 = \frac{2}{\gamma-1}\left[\left(\frac{P_{t_\infty}}{P_\infty}\right)^{\frac{\gamma-1}{\gamma}} - 1\right]$$

$$q_\infty = (1/2)\, \gamma\, P_\infty M_\infty^2$$

DATA PRESENTATION

The variation of jet Mach number M_j versus the jet momentum coefficient C_μ is shown in Figure 5 for each of the test values of free-stream Mach number. These lines are the locus of points plotted from the reduced data and, thus, reflect such influences as slot expansion with increasing duct pressure through the measured mass flow term in C_μ. The curves apply directly to this model and test configuration. Generally, the relationship will change for different slot height settings, or differences in slot expansion due to pressure.

INTEGRATED AIRFOIL COEFFICIENTS

The unblown characteristics of the airfoil are shown in Figures 6, 7, and 8 for different Mach number and angles of attack. Two trends of the lift curves are: (1) the drop in C_ℓ with increasing Mach number for constant angle of attack,

and (2) the consistently low magnitude of the lift curve slope ($\partial C_\ell/\partial\alpha$) for the unblown airfoil.

Figure 9 through 11 show airfoil characteristics versus the jet momentum coefficient. Each figure is for a given, constant Mach number but includes curves for several different angles of attack. Figure 9 shows that lift developed from blowing drops off as the C_μ exceeds a value corresponding to choked jet conditions. This closely corresponds to when Coanda surface pressures reach C_p^*. However, this is not always the case. A clear exception is shown in Figure 9d and 9e, for M_∞ = 0.6 and 0.7, where the C_ℓ continues to increase with C_μ well past the choked jet condition. Other experiments have also shown that CC airfoil operation may continue well beyond the point of a sonic jet.[7] Zero augmentation in the vicinity of choked jet flow is most likely attributable to the design of the trailing edge region. Additional transonic test data on other profiles are needed to identify the causative factors.

Drag and pitching moment data corresponding to the Figure 9 lift data are shown in Figures 10 and 11. Drag characteristics show a tendency to rise with increasing lift and then drop off after passing $C_{\ell_{max}}$. This behavior is similar to a standard lift-drag polar. Three example lift-drag polars for the NCCR 1610-8054S airfoil are shown in Figure 12 along with two NACA airfoil lift-drag polars from Abbott and von Doenhoff.[8] The CC airfoil at M = 0.3 has higher $C_{\ell_{max}}$ capability with the attendant extension in profile drag. Conversely, the CC airfoil develops a very good $C_{d_{min}}$ = 0.004 at C_ℓ = 0.55 for α = -4 deg. Similar (and lower) minimum drag values were achieved up to α = +2 deg.

Pitching moment behavior follows the C_ℓ, becoming more negative as greater suction develops on the airfoil aft upper surface. A comparison of the data in Figures 9 and 11 shows that pitching moment stall occurs near $C_{\ell_{max}}$. Closer comparison reveals that moment stall slightly precedes lift stall for angles of attack greater than -2 deg. Overall, the behavior is as expected; pitching moment at half-chord is substantially negative for negative angle of attack, and becomes more negative as jet momentum is increased.

LIFT DATA CROSS PLOTS

The variation of C_ℓ versus C_μ, as presented in Figure 9, has been cross plotted to highlight this area of interest. The cross plots (Figure 13) provide a different

perspective than that shown in Figure 9 and point out the important influence of free-stream Mach number on the CC airfoil lift capabilities.

Lift variation versus the jet momentum is presented in Figure 13 for different Mach numbers at approximately constant angle of attack. As shown in Figure 5, the C_μ range is greatly reduced for higher M_∞ (given a range of M_j). Thus, the curves of Figure 13 show much lower C_μ values for higher M_∞, which is a result of the definition of C_μ. However, the absolute value of $C_{\ell_{max}}$ is much less at higher M_∞. Currently, considerable effort is underway to define the nature of this $C_{\ell_{max}}$ and to identify the airfoil parameters which limit it. Although such an evaluation was not undertaken in the work presented, it was observed that the $C_{\ell_{max}}$ resembles a line of constant $\Delta C_{\ell_{max}} M_\infty^2$. This corresponds to a condition of constant Δ lift force available from jet augmentation over the free-stream Mach range.

Maximum values of lift due to blowing ($\Delta C_\ell \equiv C_{\ell_{max}} - C_{\ell_o}$) are plotted versus free-stream Mach number for several angles of attack in Figure 14. These curves show the characteristic drop in maximum augmented lift as Mach number increases. Also noticeable is the influence of angle of attack on the maximum ΔC_ℓ — an important characteristic since the CC airfoils usually operate at negative angles in a rotor application; see Reference 1 for typical operational ranges. The curves in Figure 14 show the approximate upper limit of lift capability as a function of both Mach number and geometric angle of attack.

SURFACE PRESSURE COEFFICIENTS

The distribution of surface pressure coefficient C_p shows some flow characteristics of the airfoil. Figures 15 and 16 are included to exemplify the changes in airfoil C_p distribution as Mach number and C_μ vary. Figures 15a and 15b show C_p distribution as C_μ is increased. Figure 15a shows the powerful influence of the blowing jet dramatically altering the C_p distribution at $M_\infty = 0.30$, thereby directly controlling C_ℓ. Similar influence is observed at $M = 0.5$ in Figure 15b, but diminishes as the wall jet approaches C_p^*.

Figures 16a and 16b show C_p distributions as M_∞ is increased for fixed blowing and angle of attack. Figure 16a shows the unblown airfoil ($M_j = 0$, $C_\mu = 0$) at constant $\alpha = -2$ deg. This corresponds to the lift variation shown in Figure 6. Figure 16b shows the C_p distributions for constant jet Mach number $M_j = 0.89$ at

α = -4 deg. The value of M_j is high enough to exhibit augmented characteristics but is below any stall region. The value was chosen to be representative of typical CC airfoil C_p distributions.

CONCLUDING REMARKS

The NCCR 1610-8054S airfoil profile exhibited characteristics which satisfied the CC airfoil development program objectives of achieving improved performance at transonic speeds while maintaining high-lift augmentation at low subsonic speeds.

1. High-lift capability was demonstrated at low subsonic speeds, while extending the Mach number range for effective direct lift control up to M_∞ = 0.7. These combined attributes were not previously available from any single CC airfoil.

2. Maximum lift coefficient at zero-deg angle of attack varies from 2.0 at M_∞ = 0.3 to 0.35 at M_∞ = 0.7. The variation resembles a $1/M_\infty^2$ curve, which corresponds to a constant lift force versus M_∞. Nominally, the variation would appear to be a desirable trait, as it represents a nearly constant aerodynamic force capability over a broad Mach range. This further suggests nearly constant aerodynamic lift sensitivity to the percent of blowing control used.

3. The test data have established previously unknown influences of angle of attack on the maximum obtainable C_ℓ. Most significant is the expected affect of lift curve slope ($\partial C_\ell / \partial \alpha$) for the unblown airfoil. Negative angles of attack produce a negative bias on the C_{ℓ_o} value, especially at higher subsonic M_∞. However, angle of attack also influences the maximum available augmented lift ($\Delta C_\ell = C_{\ell_{max}} - C_{\ell_o}$) for all M_∞ values tested. More negative angles of attack yield noticably less ΔC_ℓ from the tested CC profile.

4. At low subsonic Mach numbers, the profile drag tends to follow a rather conventional lift-drag polar, which compares favorably to that of a selected NACA airfoil section. Values of $C_{d_{min}}$ change according to M_∞, α, and C_μ. At M_∞ = 0.3, minimum drag coefficients of 0.0032 to 0.0051 were measured for the C_ℓ range of 0.45 to 0.60. Values of $C_{d_{min}}$ generally increased with increasing M_∞.

5. Pitching moment coefficients were resolved about the 50-percent chord. The variation was as expected: $C_{m_{50}}$ decreased as angle of attack decreased, and became more negative as jet momentum was increased. At low M_∞, C_μ has a greater

influence on $C_{m_{50}}$ than α; while at higher M_∞, α has the greater influence.

Overall, the transonic test data presented are more comprehensive than any previous results on CC airfoils with respect to the significance of angle of attack on airfoil performance. Nevertheless, the experimental nature of the spiral trailing edge geometry should be recognized. While this geometry has provided good augmentation, it is far from optimum in terms of profile drag (jet thrust recovery). Further refinements of the bluff trailing edge of CC airfoils should lead to higher M_{crit}, improved drag, and even greater lift capability.

ACKNOWLEDGMENT

The authors would like to recognize the following individuals for their participation and contributions to the program:

J.S. Abramson
D.R. Chaddock
A.P. Clark
S.M. Gottlieb
W.B. Maguire
F.R. Ridley
E.O. Rogers
A.A. Rok

REFERENCES

1. Wilkerson, J.B., "An Assessment of Circulation Control Airfoil Development," DTNSRDC Report 77-0084 (Aug 1977).
2. Abramson, J., "Two-Dimensional Subsonic Wind Tunnel Evaluation of Two Related 15-Percent Thick Circulation Control Airfoils," DTNSRDC ASED Report 373 (Sep 1977).
3. Abramson, J., "The Low Speed Characteristics of a 15-Percent Quasi-Elliptical Circulation Control Airfoil with Distributed Camber," Report DTNSRDC/ASED-79/07 (May 1979).
4. Clark, A.P., "Design of a Circulation Control Airfoil Model for Evaluation in the Transonic Wind Tunnel," DTNSRDC Report CID-77-1 (Mar 1977).
5. ASED Staff, "Transonic Wind-Tunnel Facility at the Naval Ship Research and Development Center," DTNSRDC Report ASED-332, (Jun 1975).
6. Schlichting, H., "Boundary Layer Theory," Sixth Edition, McGraw-Hill Book Company, New York (1968) pp. 708-713.
7. Englar, R.J., "Experimental Investigation of the High Velocity Coanda Wall Jet Applied to Bluff Trailing Edge Circulation Control Airfoils," DTNSRDC Report 4708 (Sep 1975).
8. Abbott, I.H. and A.E. von Doenhoff, "Theory of Wing Sections," Dover Publications, New York (1959).

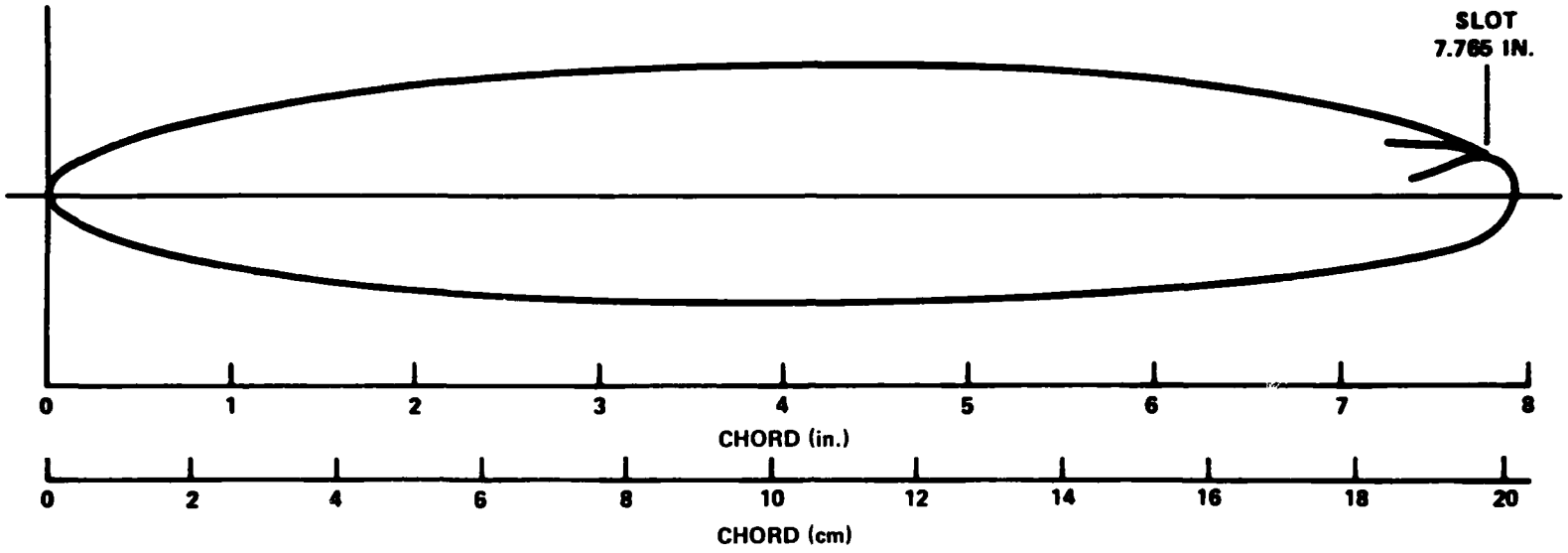

Figure 1a - Airfoil Contour

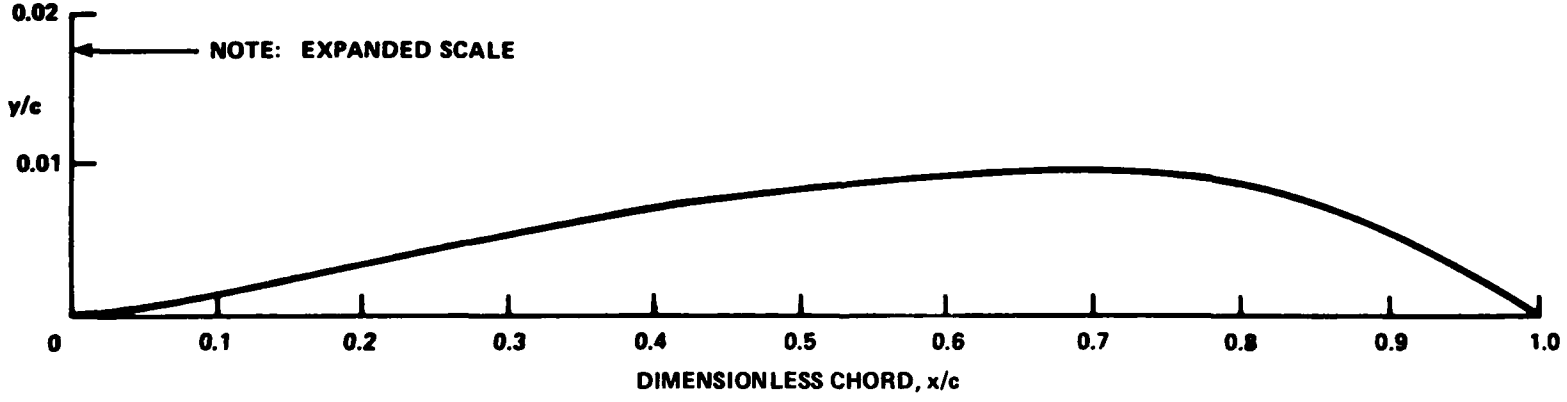

Figure 1b - Camber Distribution

Figure 1 - Contour and Camber for NCCR 1610-8054S Airfoil

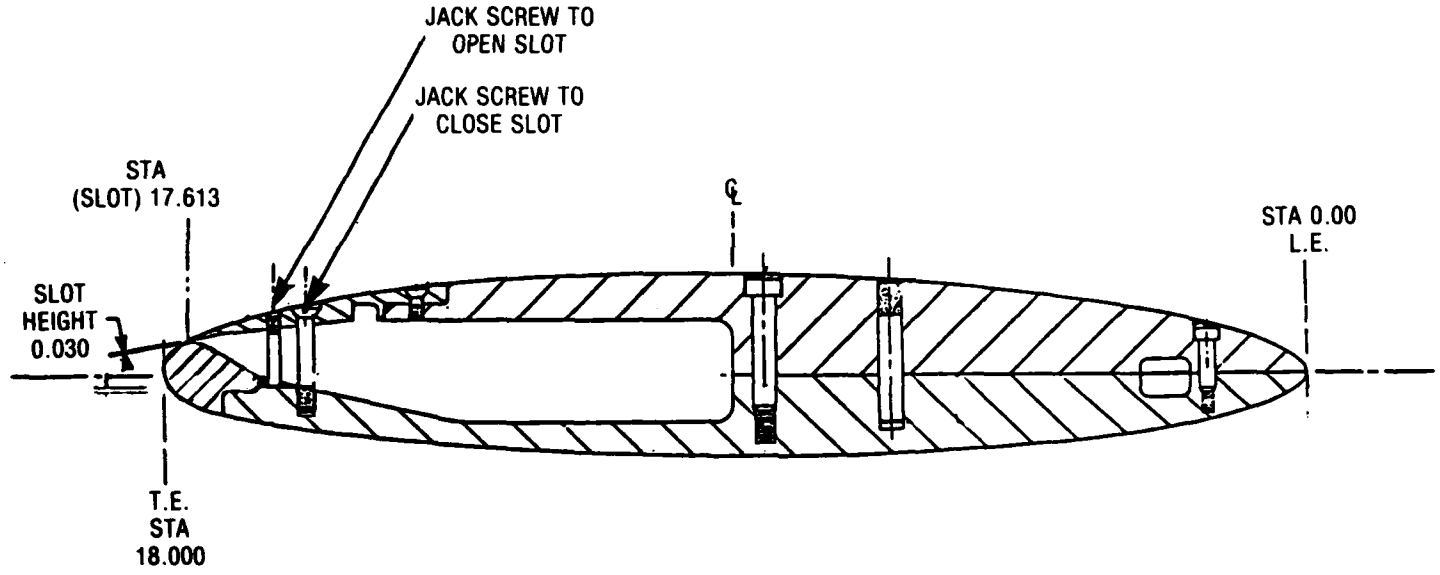

NOTE: ALL DIMENSIONS ARE IN INCHES.

Figure 2 - Model Cross-Section Details

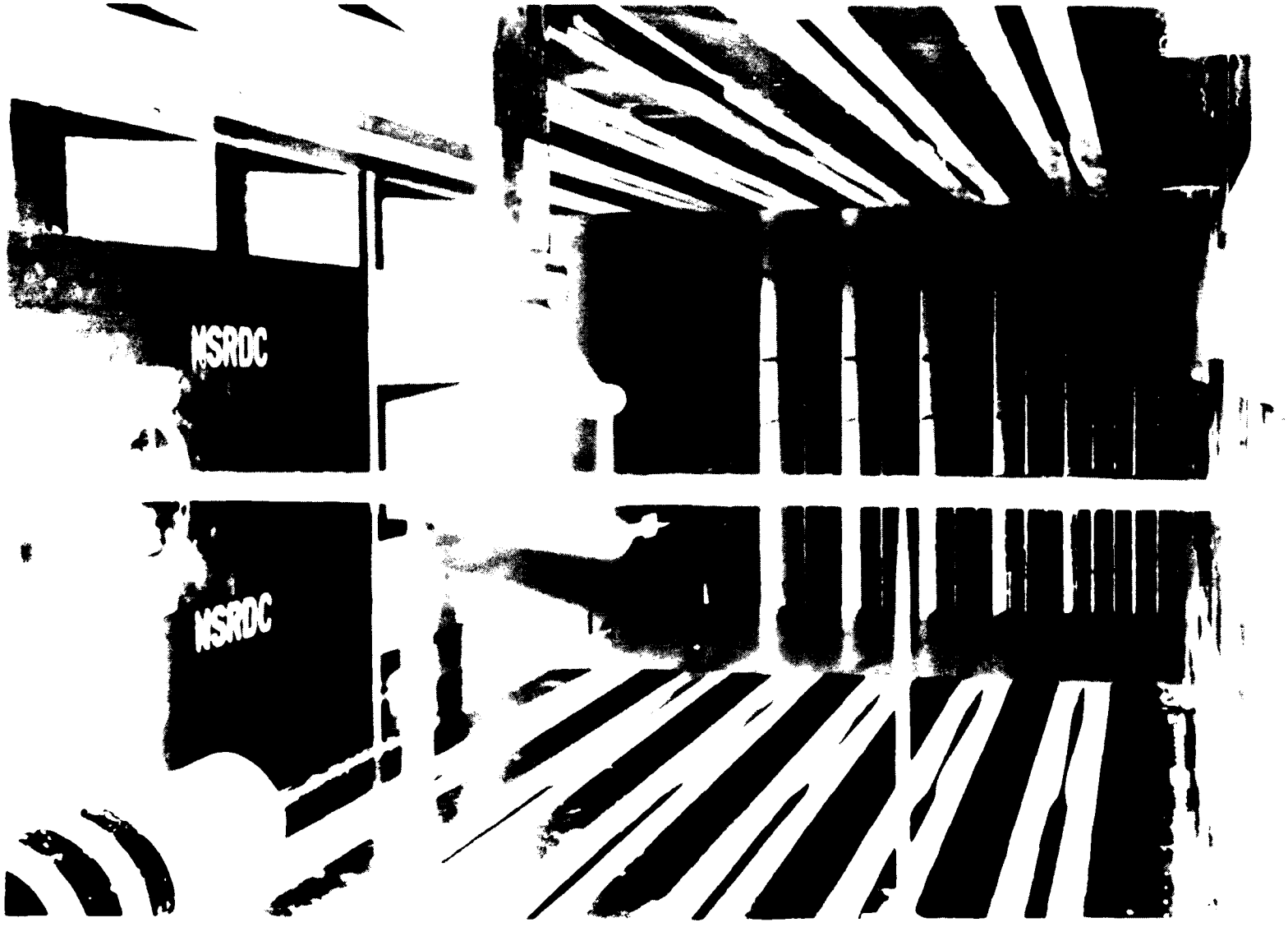

Figure 3 - Two-Dimensional CC Airfoil Installed in the DTNSRDC 7- by 10-Foot Transonic Wind Tunnel (Looking Upstream)

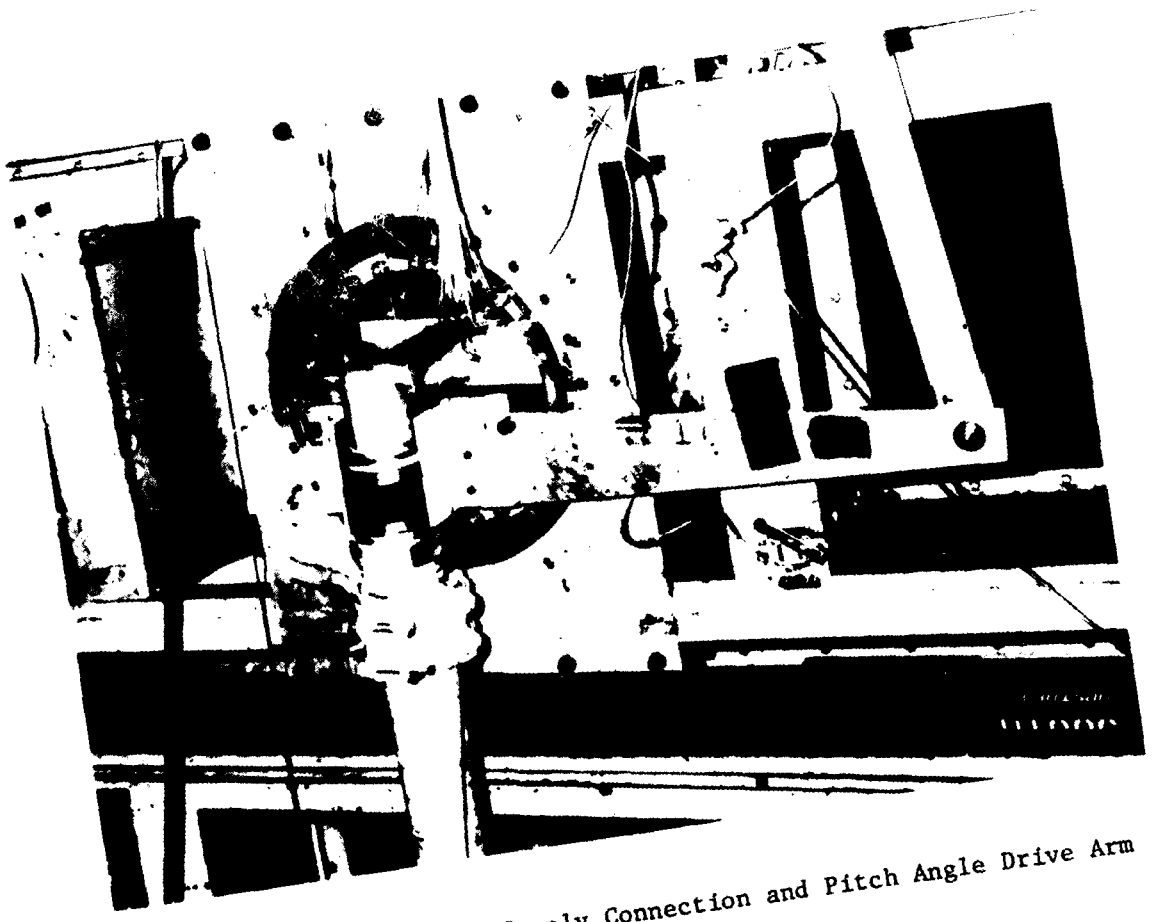

Figure 4 - External Air Supply Connection and Pitch Angle Drive Arm

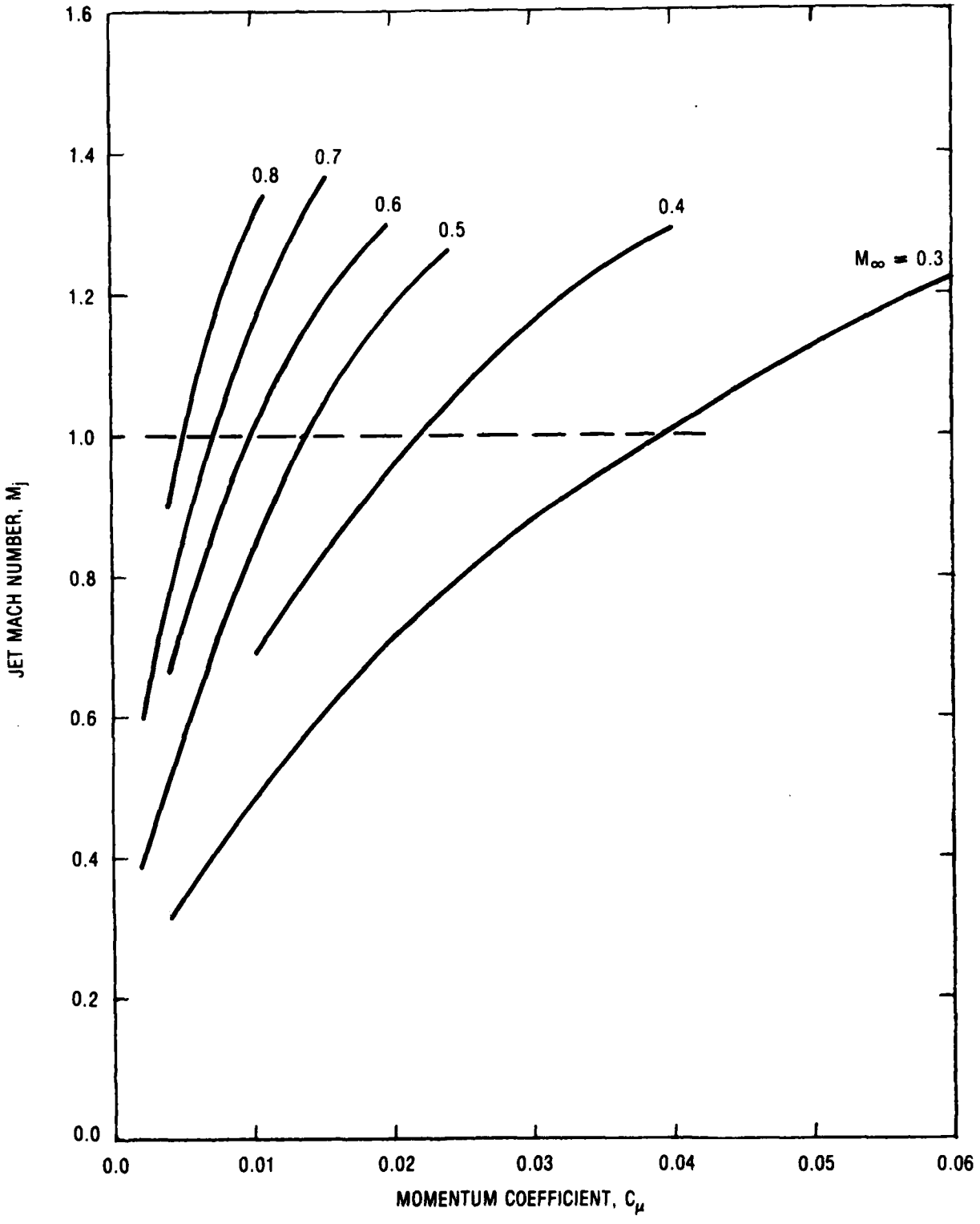

Figure 5 - Relation Between Jet Mach Number and Momentum Coefficient

Figure 6 - Lift Variation for the Unblown Airfoil

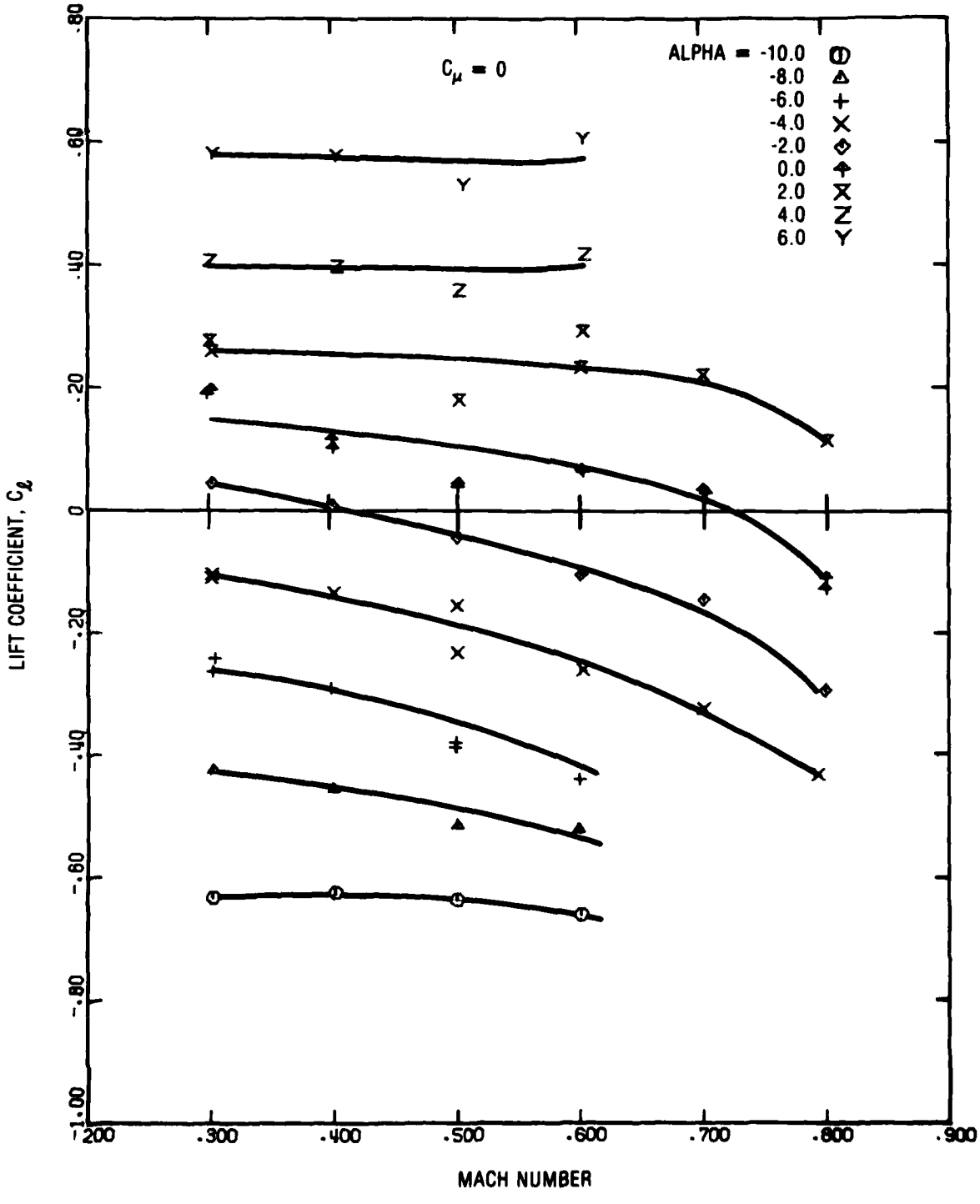

Figure 6a - Lift Coefficient versus Mach Number

Figure 6 (Continued)

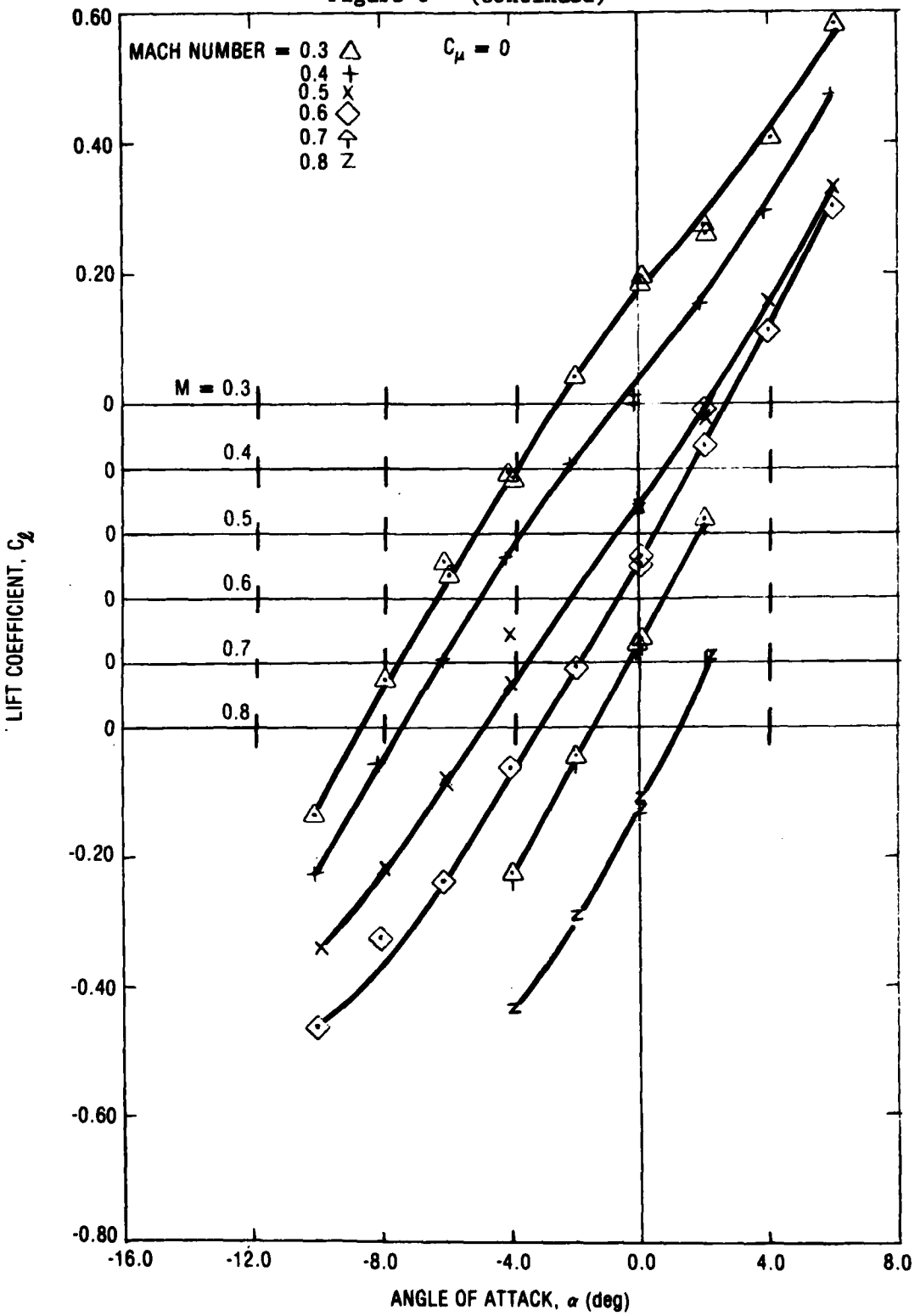

Figure 6b - Lift Coefficient versus Angle of Attack

Figure 7 - Drag Variation for the Unblown Airfoil

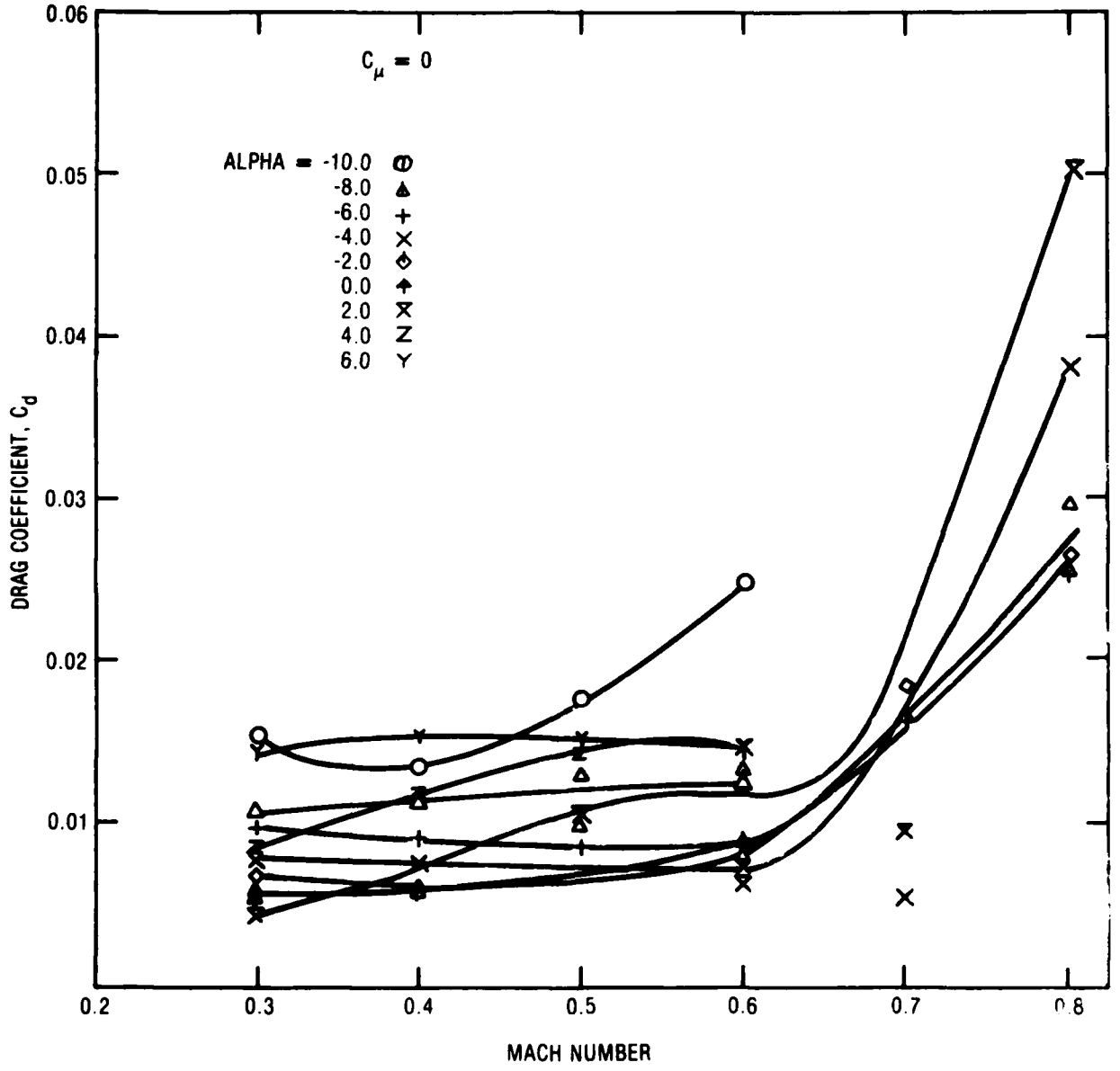

Figure 7a - Drag Coefficient versus Mach Number

Figure 7 (Continued)

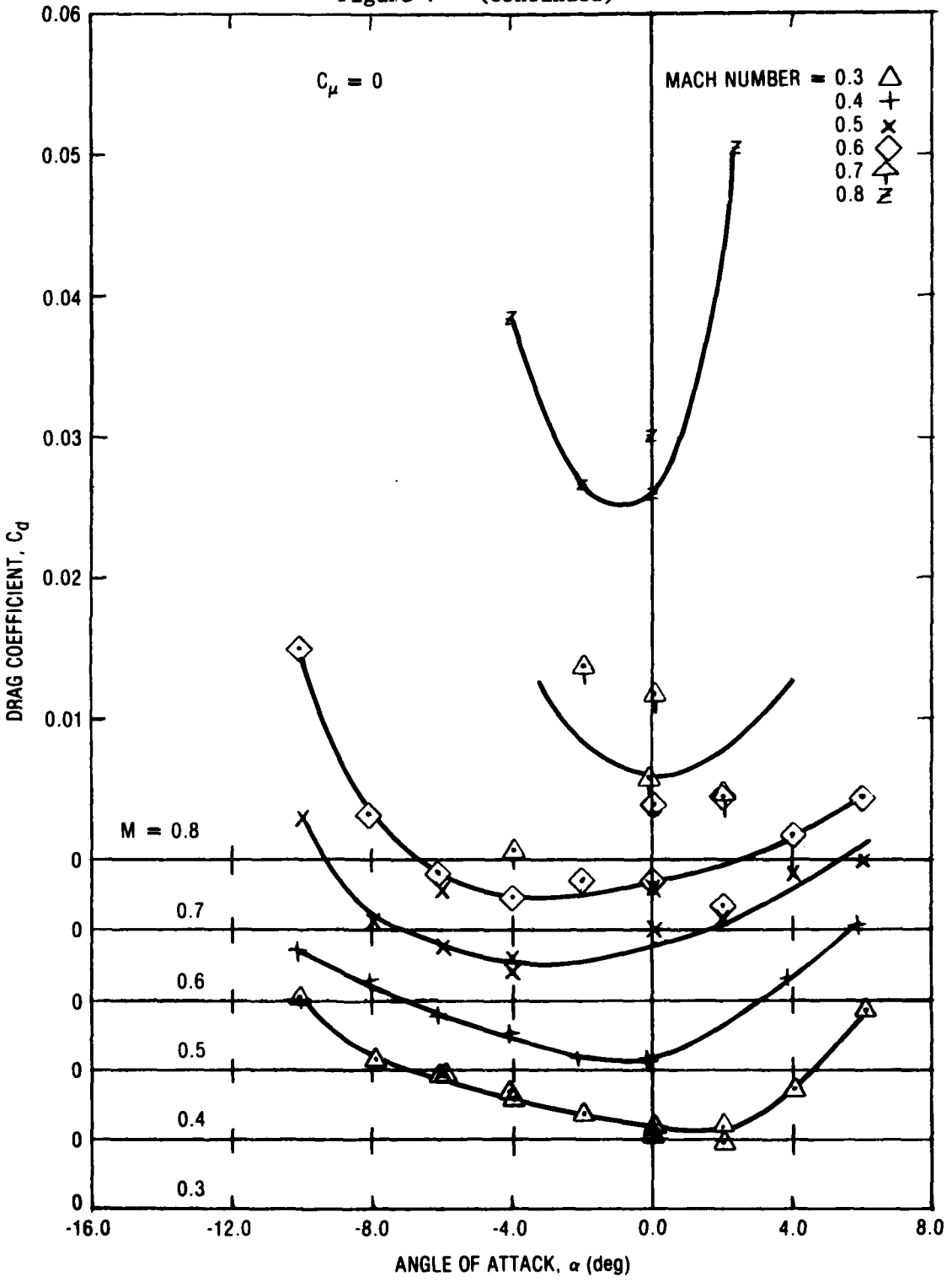

Figure 7b - Drag Coefficient versus Angle of Attack

Figure 8 - Pitching Moment Variation for the Unblown Airfoil

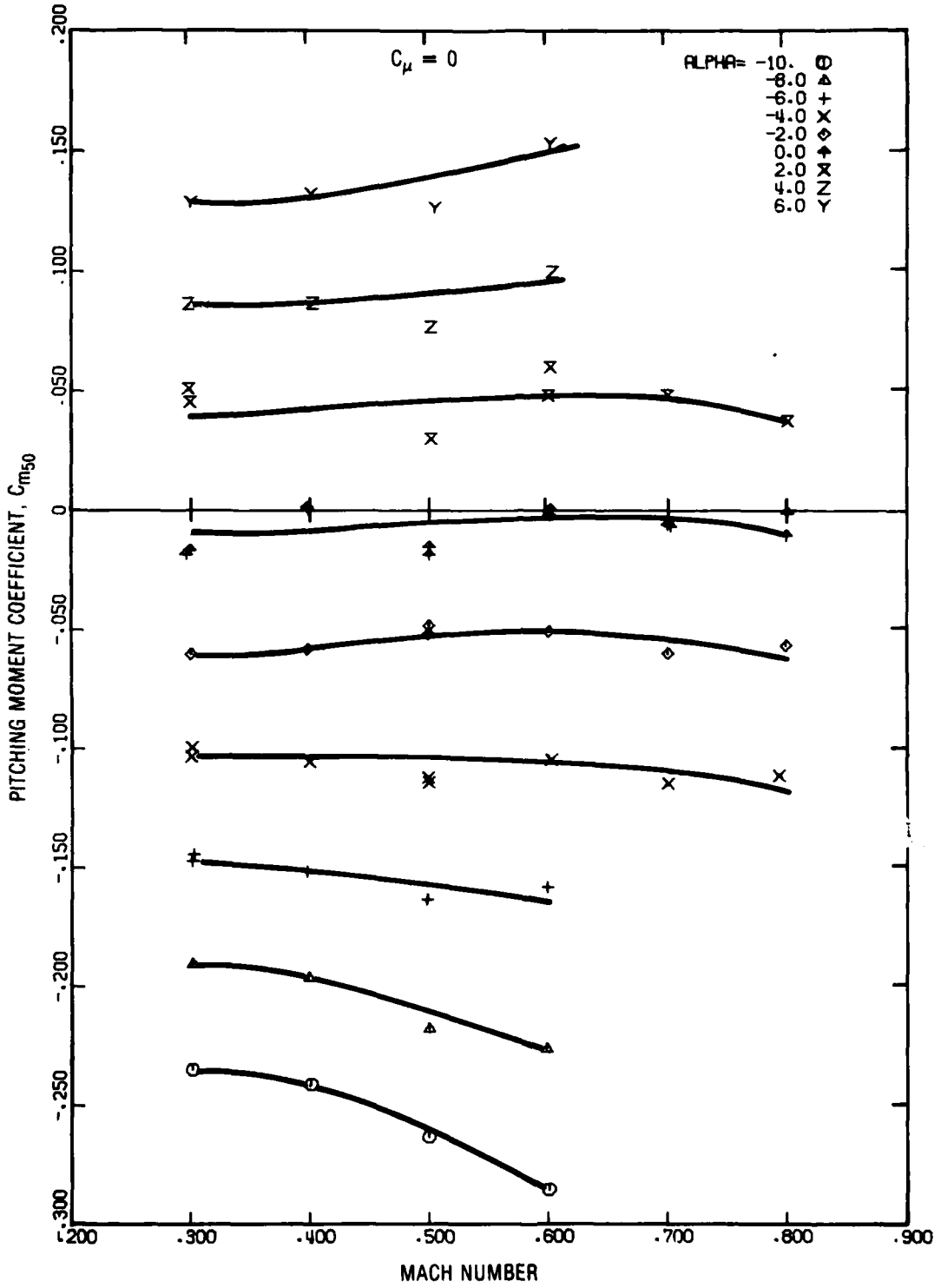

Figure 8a - Moment Coefficient versus Mach Number

Figure 8 (Continued)

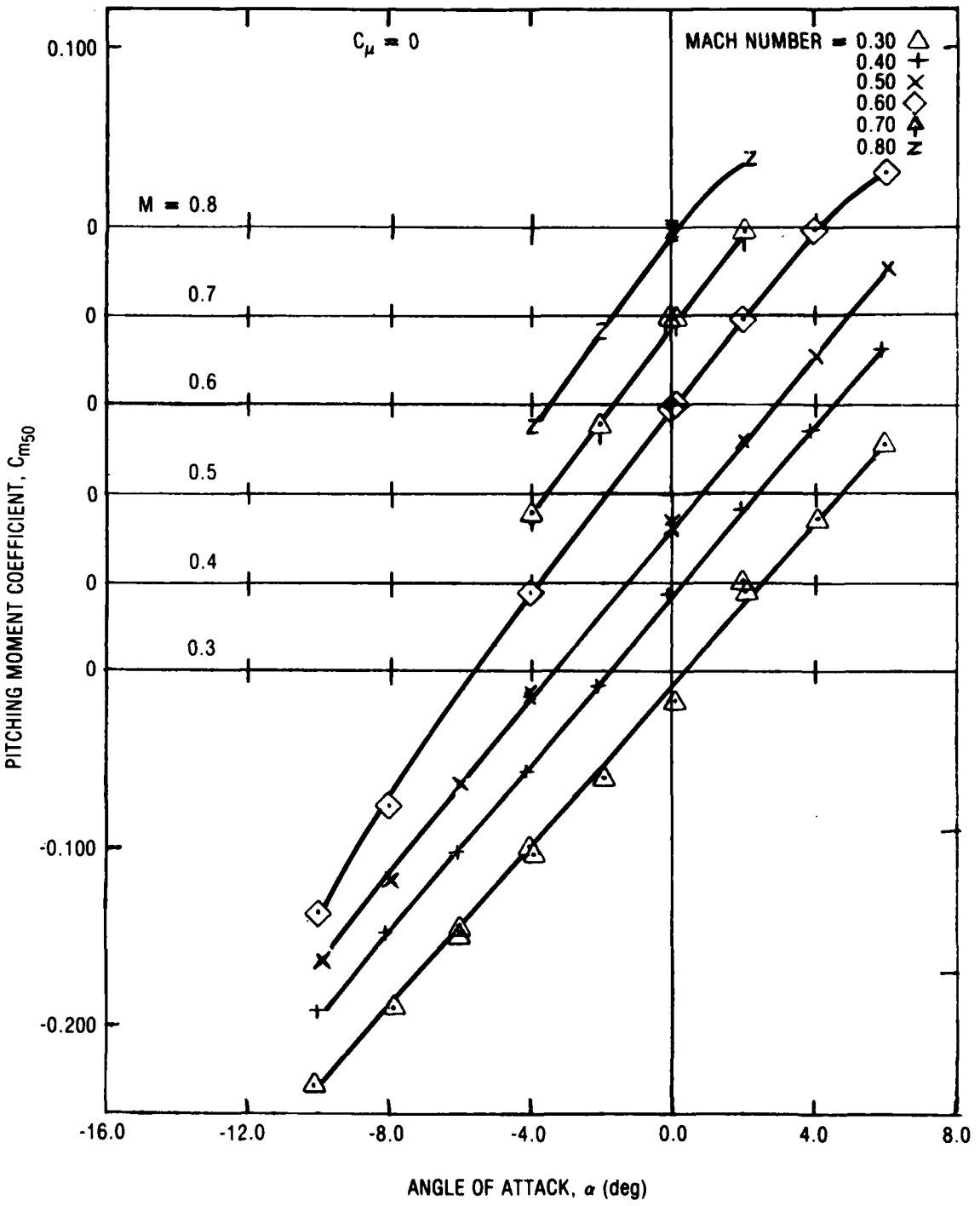

Figure 8b - Moment Coefficient versus Angle of Attack

Figure 9 - Lift Variation with Jet Momentum for Constant Mach Number

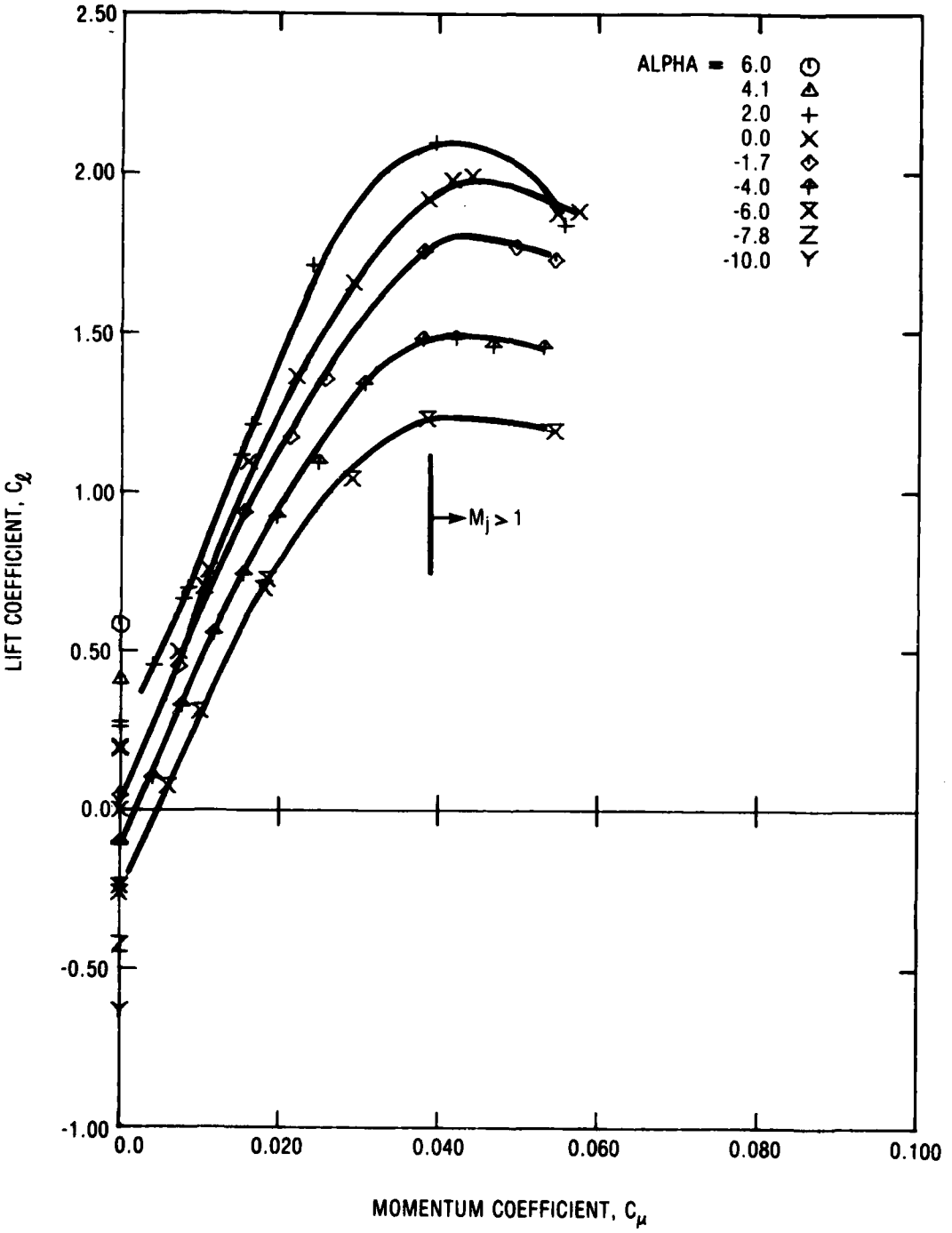

Figure 9a - Mach Number = 0.3

Figure 9 (Continued)

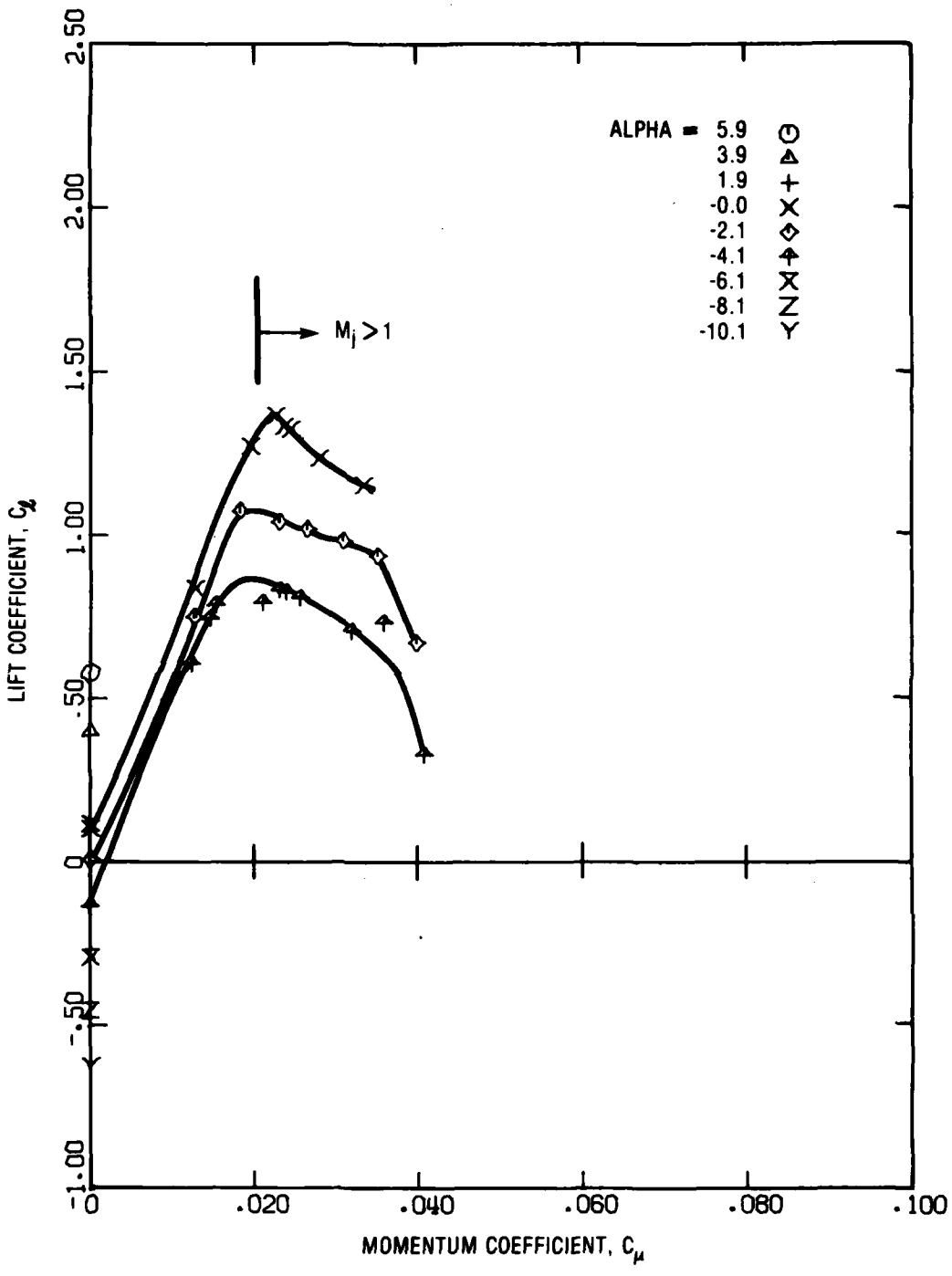

Figure 9b - Mach Number = 0.4

Figure 9 (Continued)

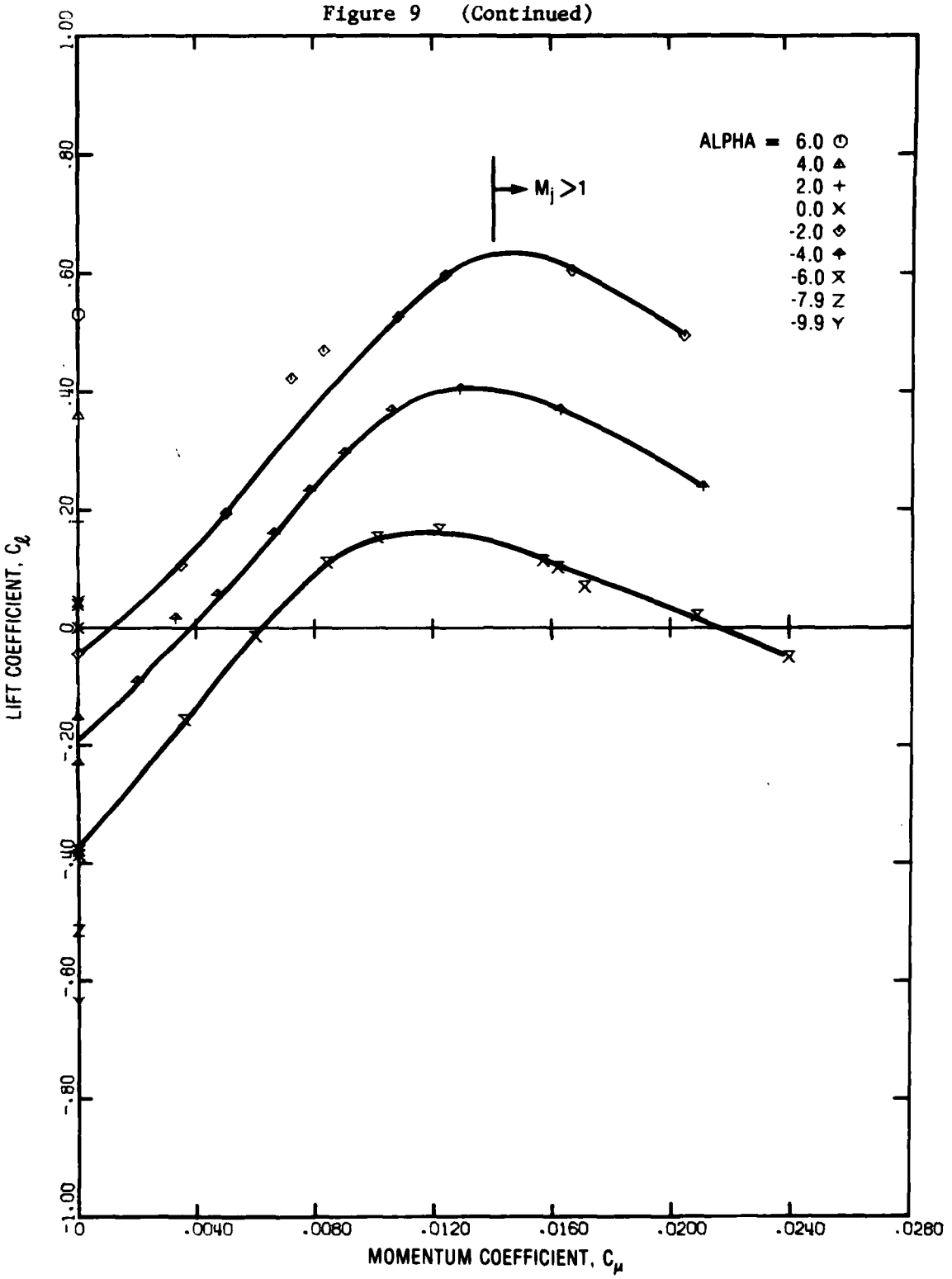

Figure 9c - Mach Number = 0.5

Figure 9 (Continued)

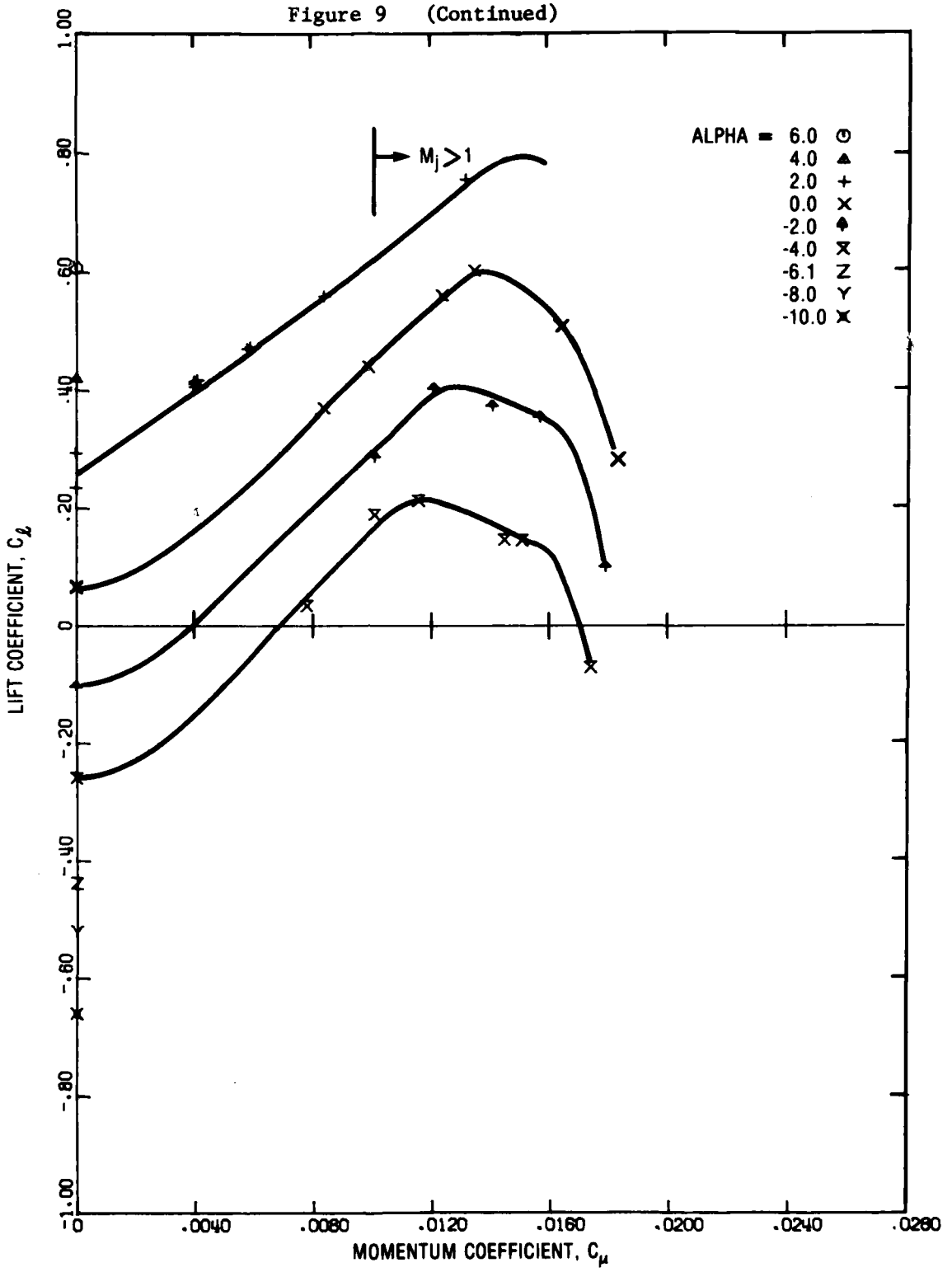

Figure 9d - Mach Number = 0.6

Figure 9 (Continued)

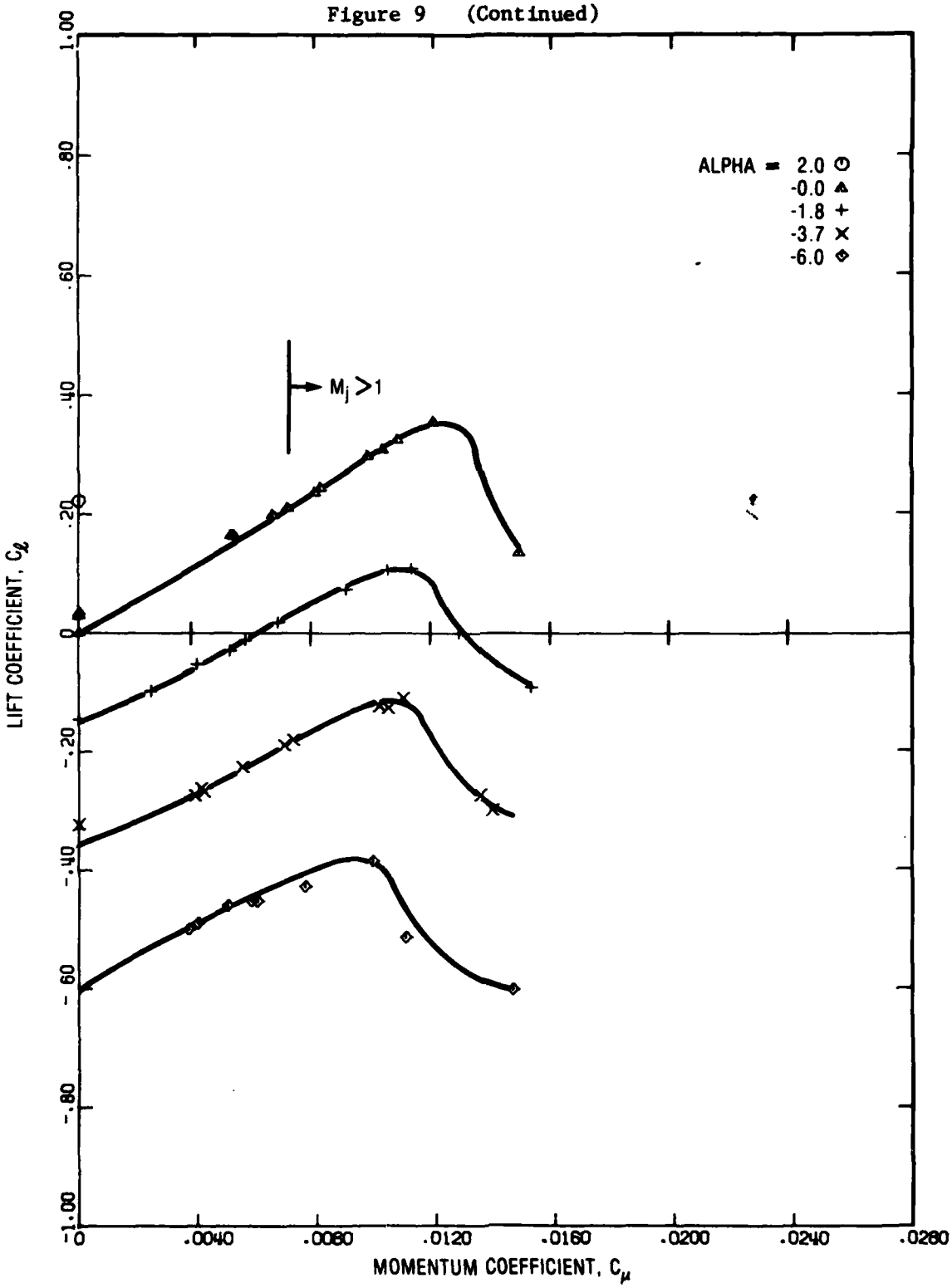

Figure 9e - Mach Number = 0.7

Figure 9 (Continued)

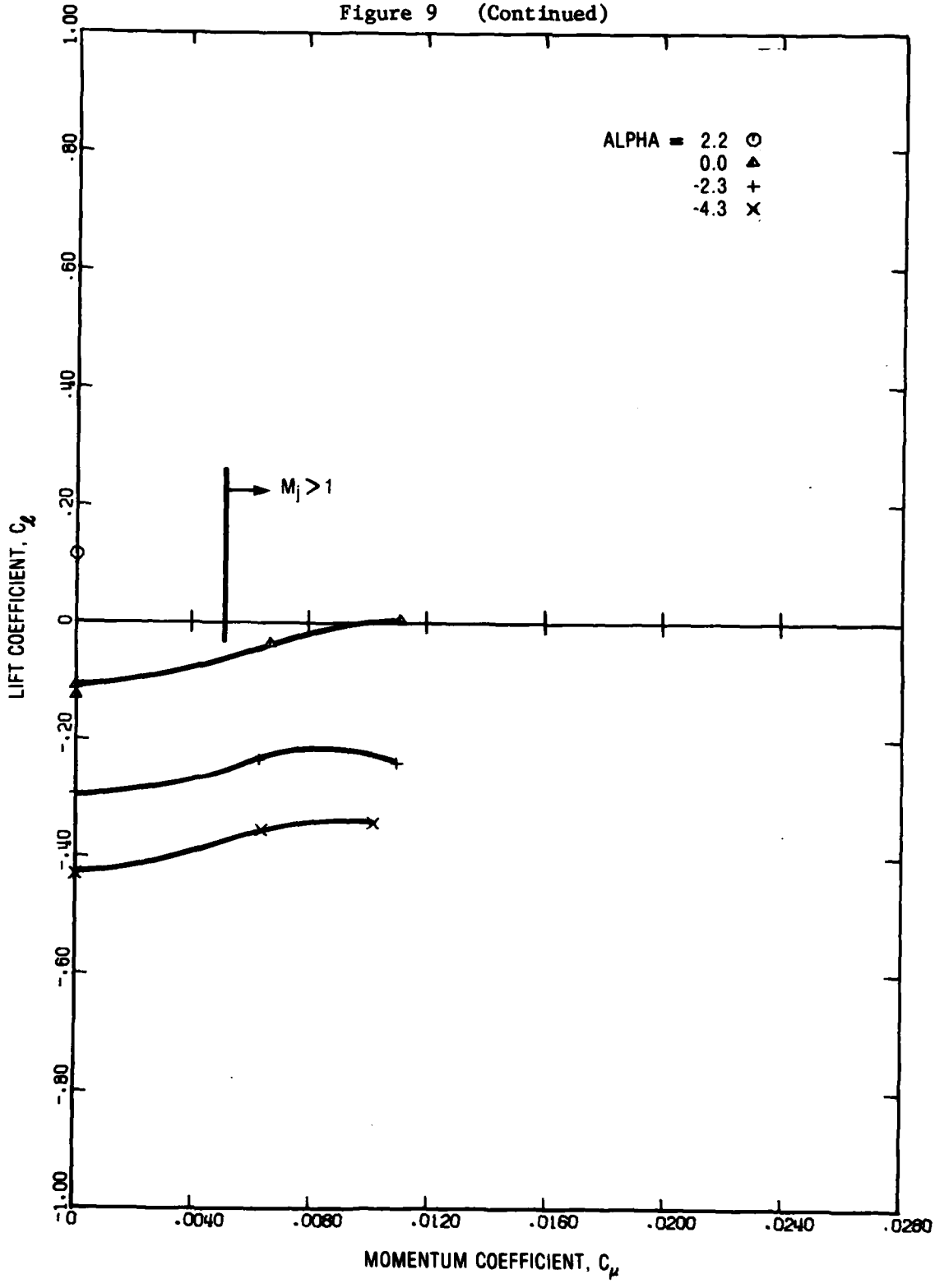

Figure 9f - Mach Number = 0.8

Figure 10 - Drag Variation with Jet Momentum for Constant Mach Number

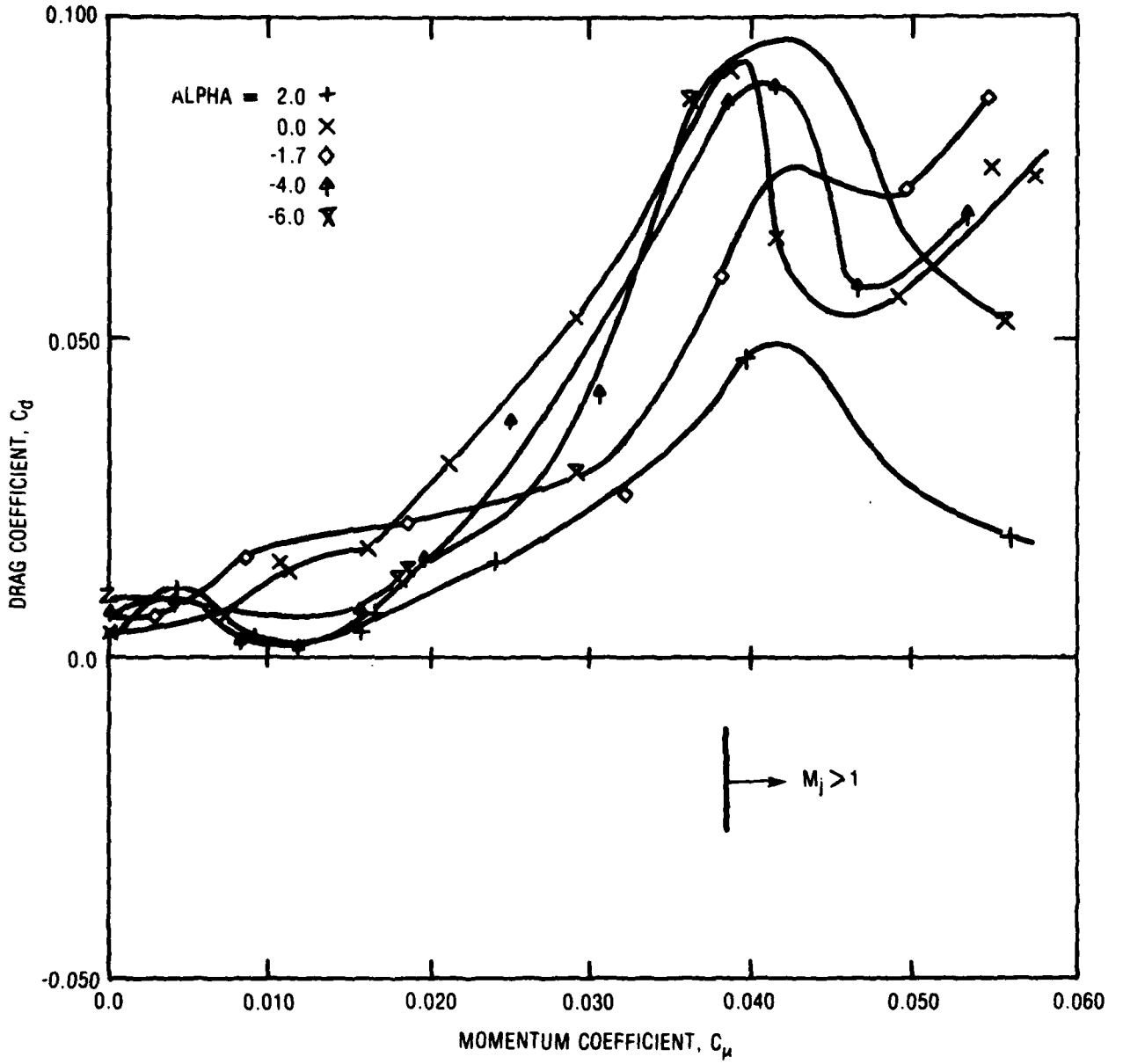

Figure 10a - Mach Number = 0.3

Figure 10 (Continued)

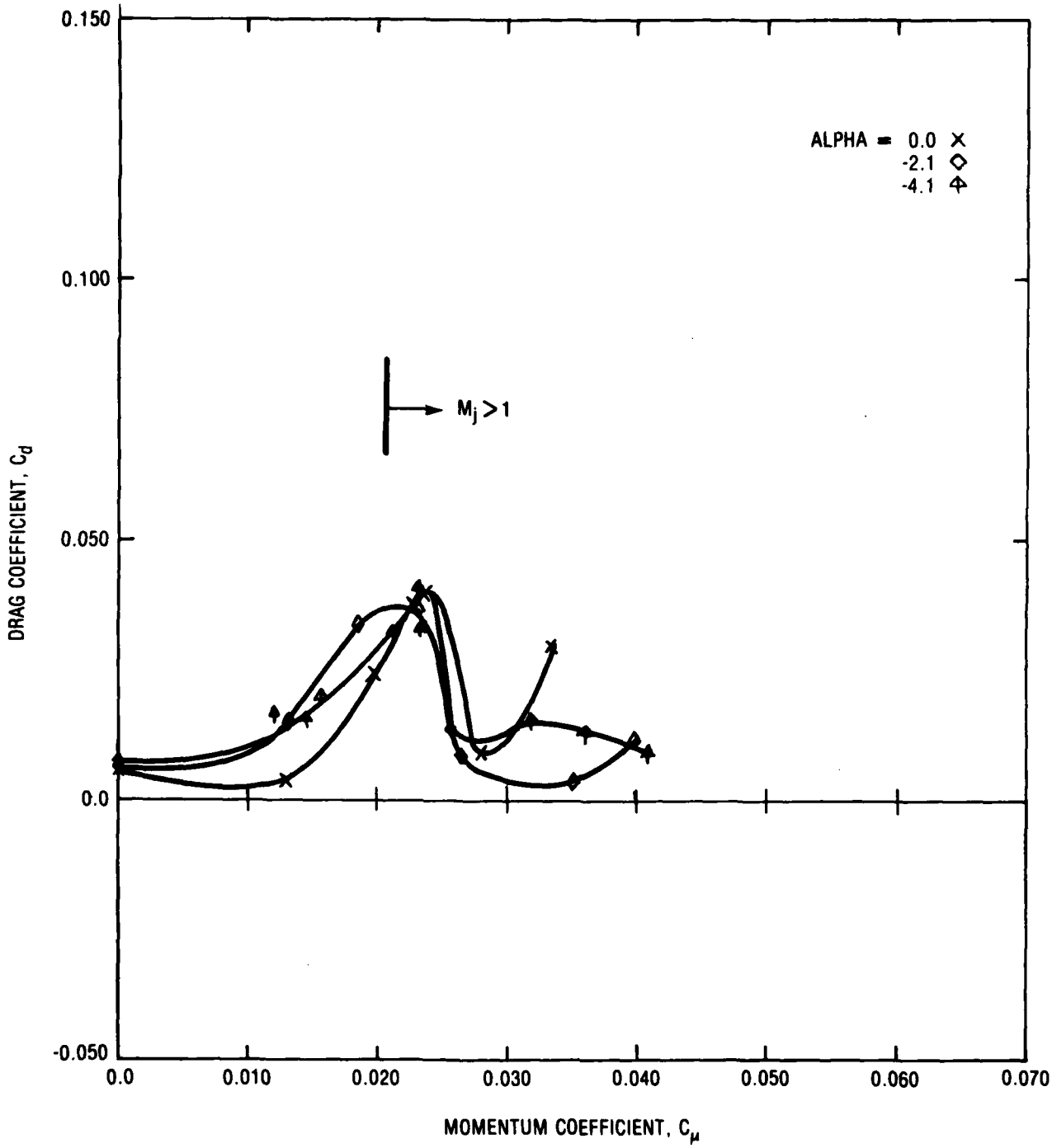

Figure 10b - Mach Number = 0.4

Figure 10 (Continued)

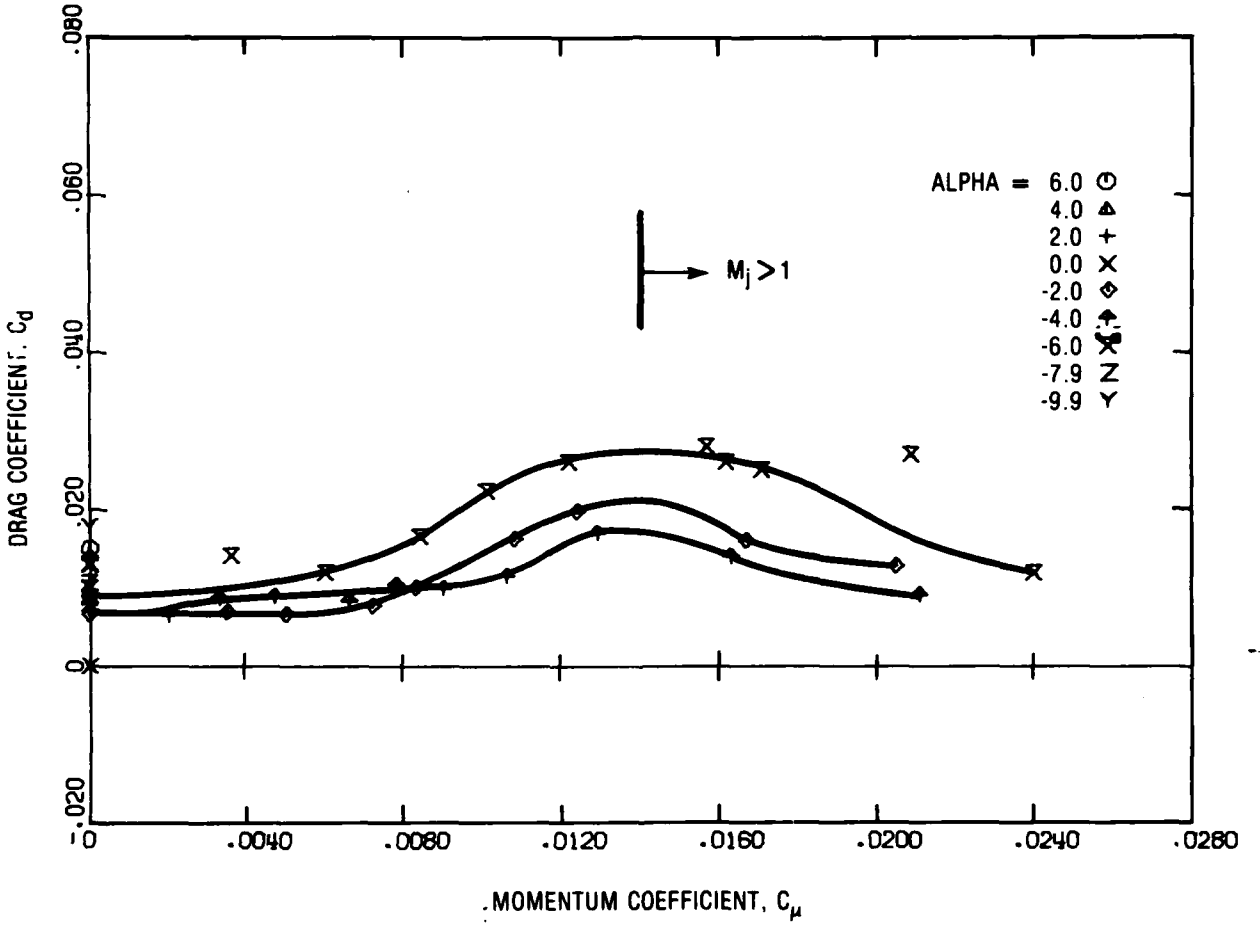

Figure 10c - Mach Number = 0.5

Figure 10 (Continued)

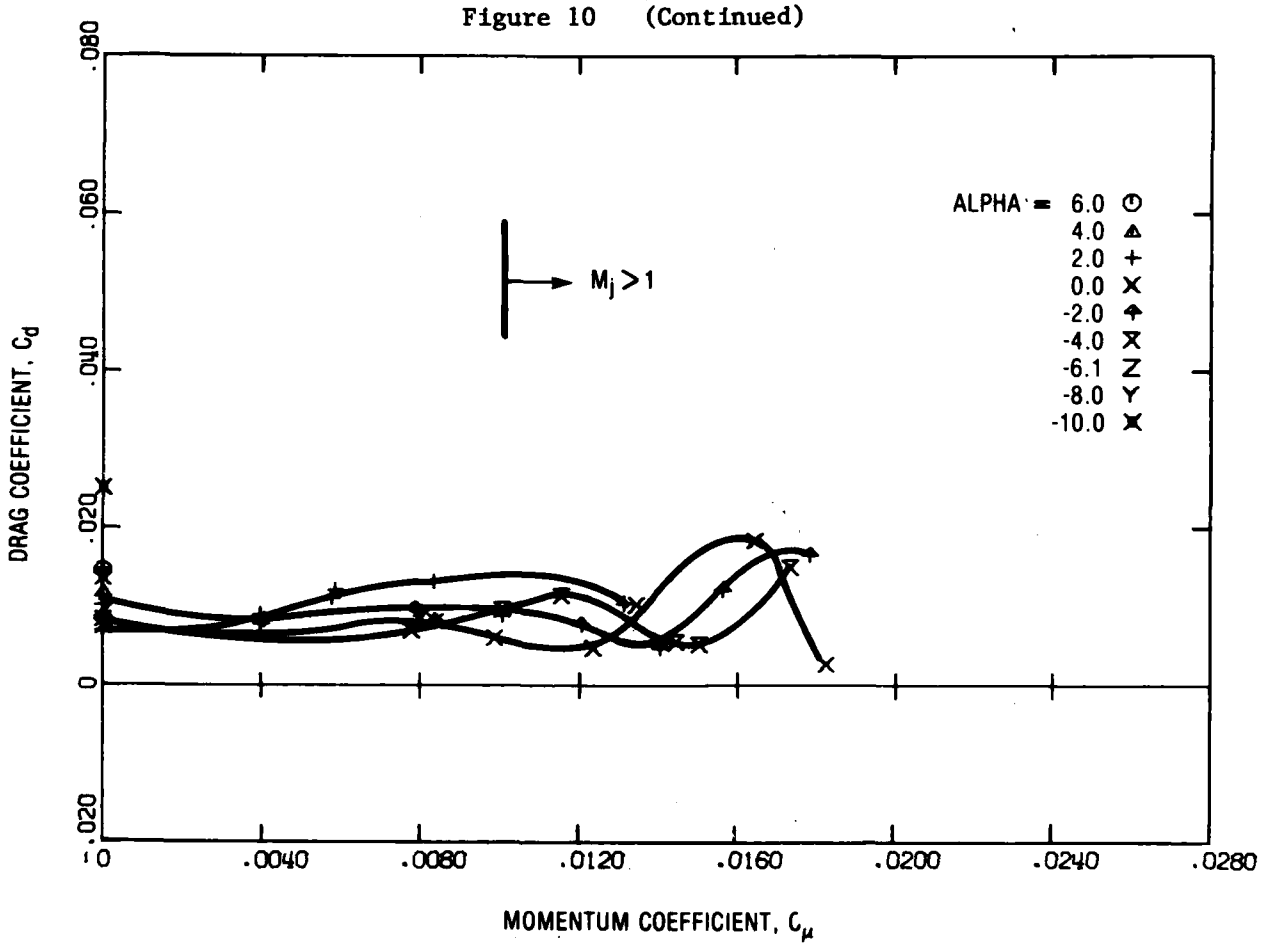

Figure 10d - Mach Number = 0.6

Figure 10 (Continued)

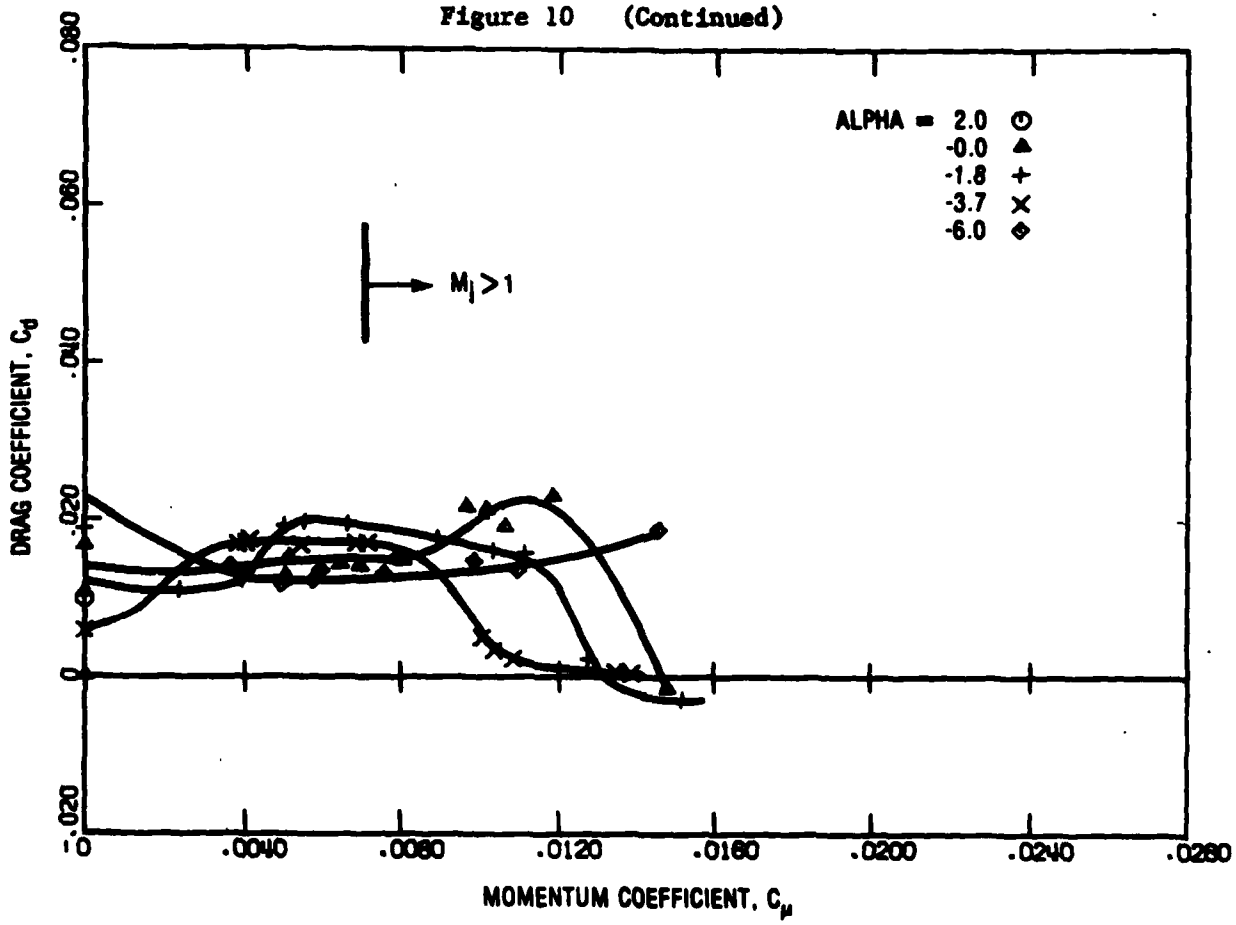

Figure 10e - Mach Number = 0.7

Figure 10 (Continued)

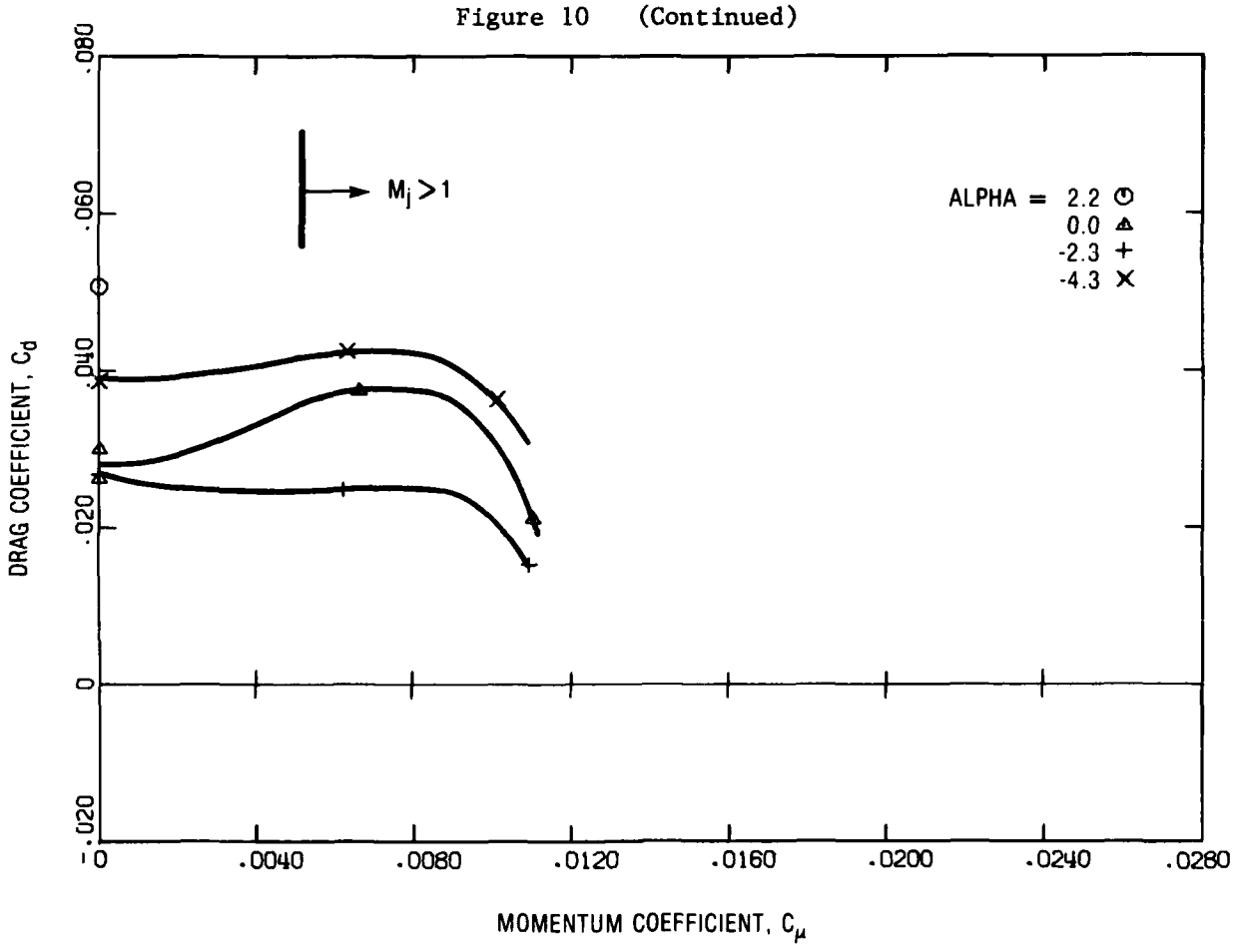

Figure 10f - Mach Number = 0.8

Figure 11 - Pitching Moment Variation with Jet Momentum for Constant Mach Number

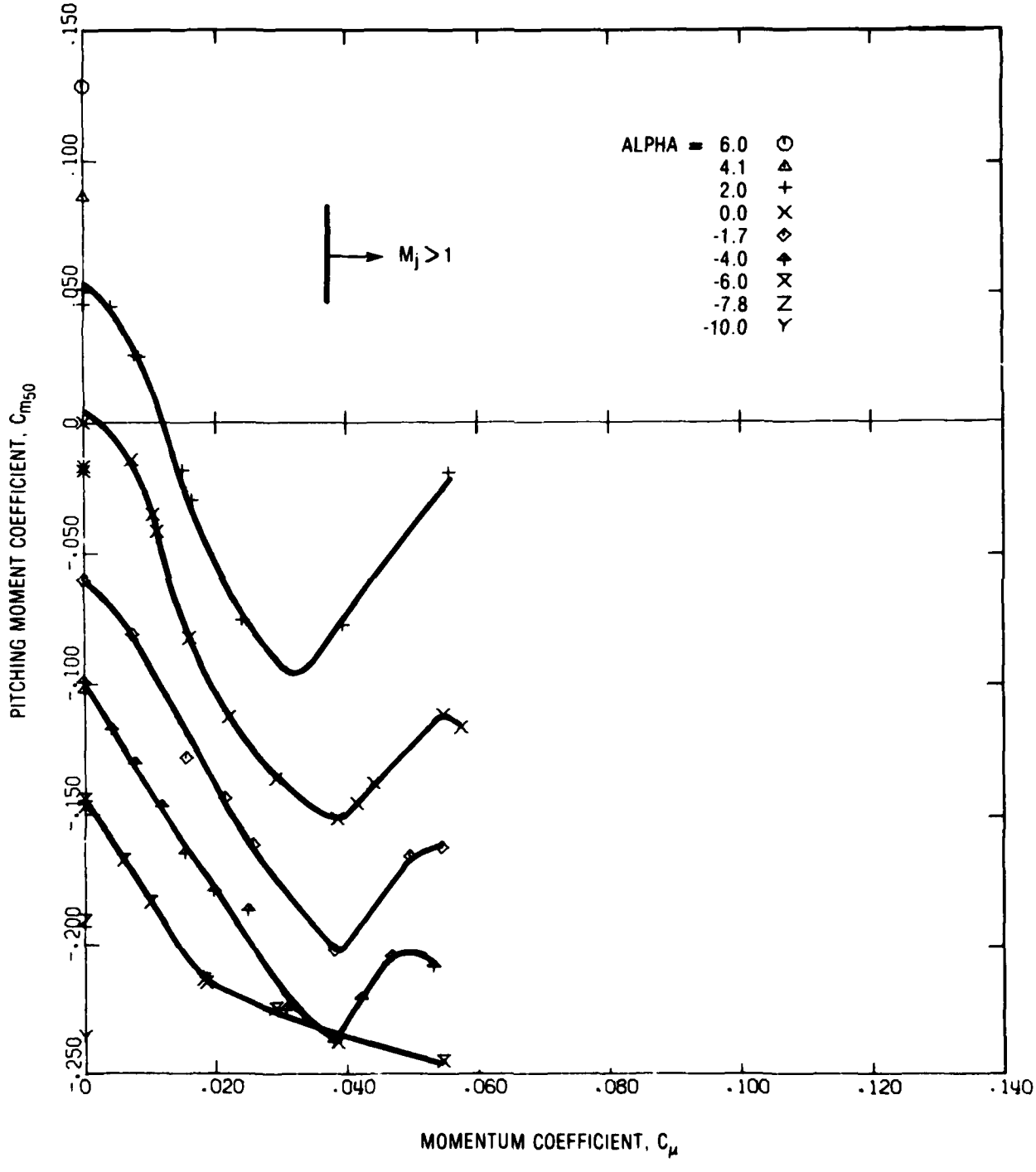

Figure 11a - Mach Number = 0.3

Figure 11 (Continued)

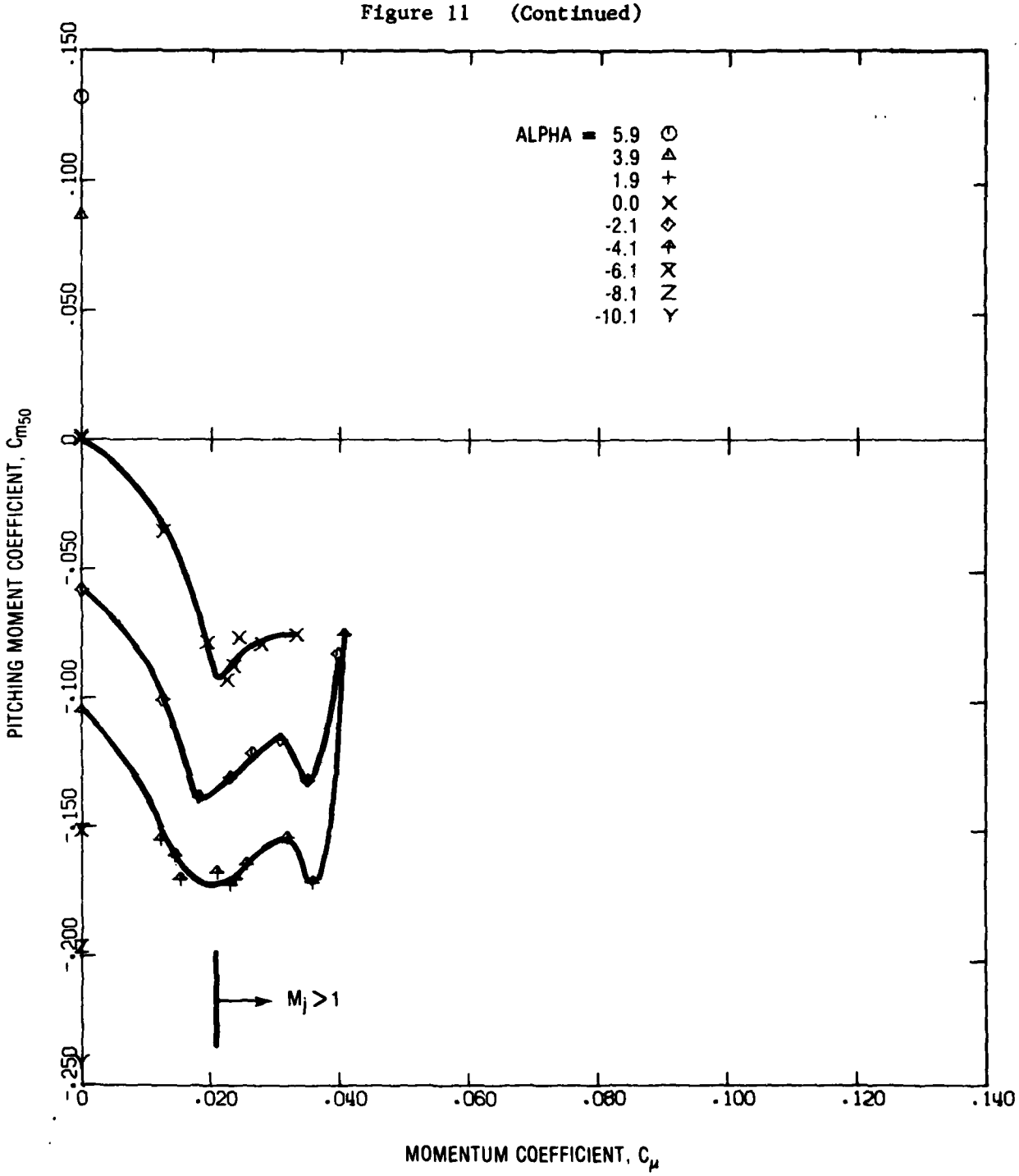

Figure 11b - Mach Number = 0.4

Figure 11 (Continued)

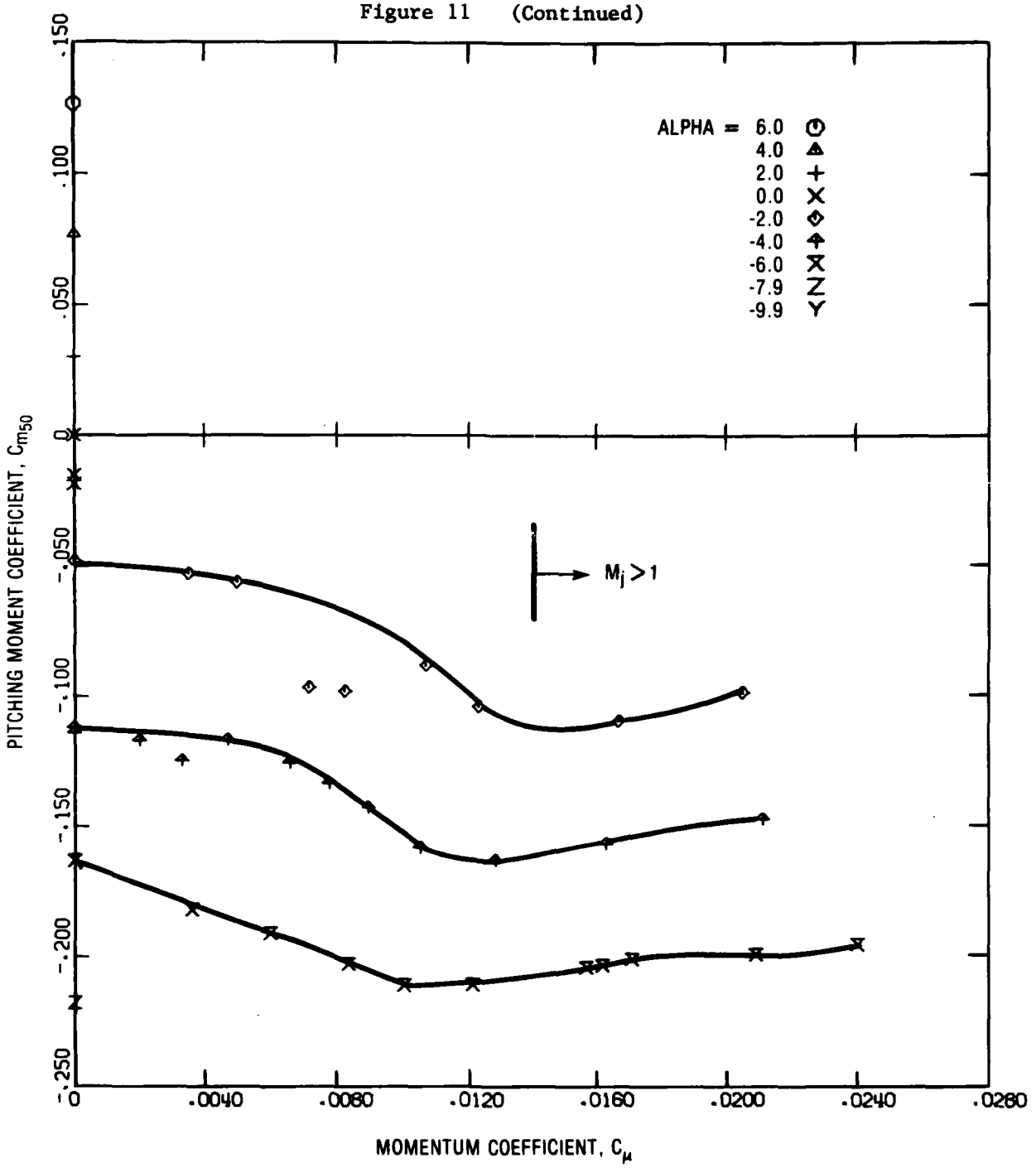

Figure 11c - Mach Number = 0.5

Figure 11 (Continued)

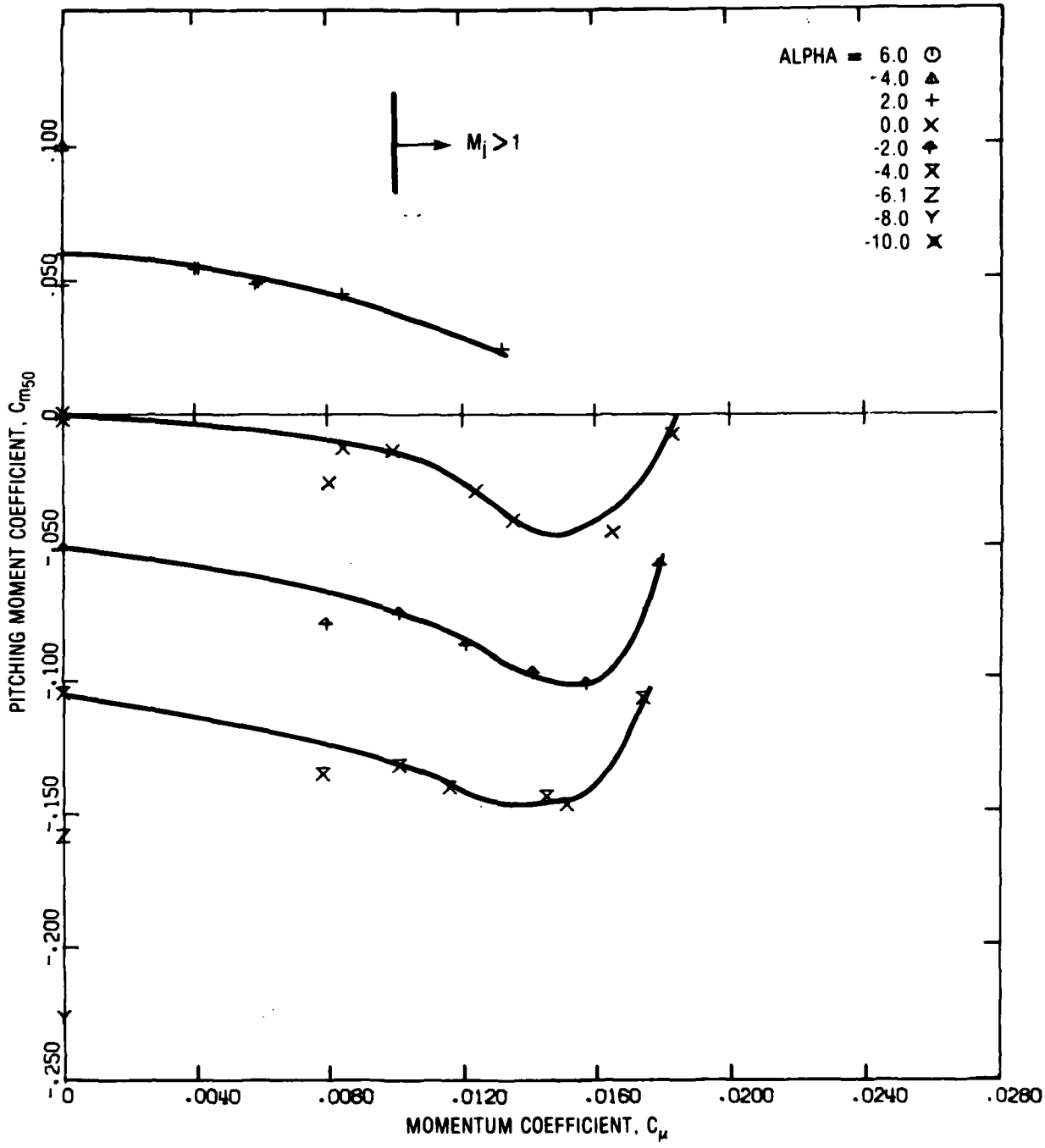

Figure 11d - Mach Number = 0.6

Figure 11 (Continued)

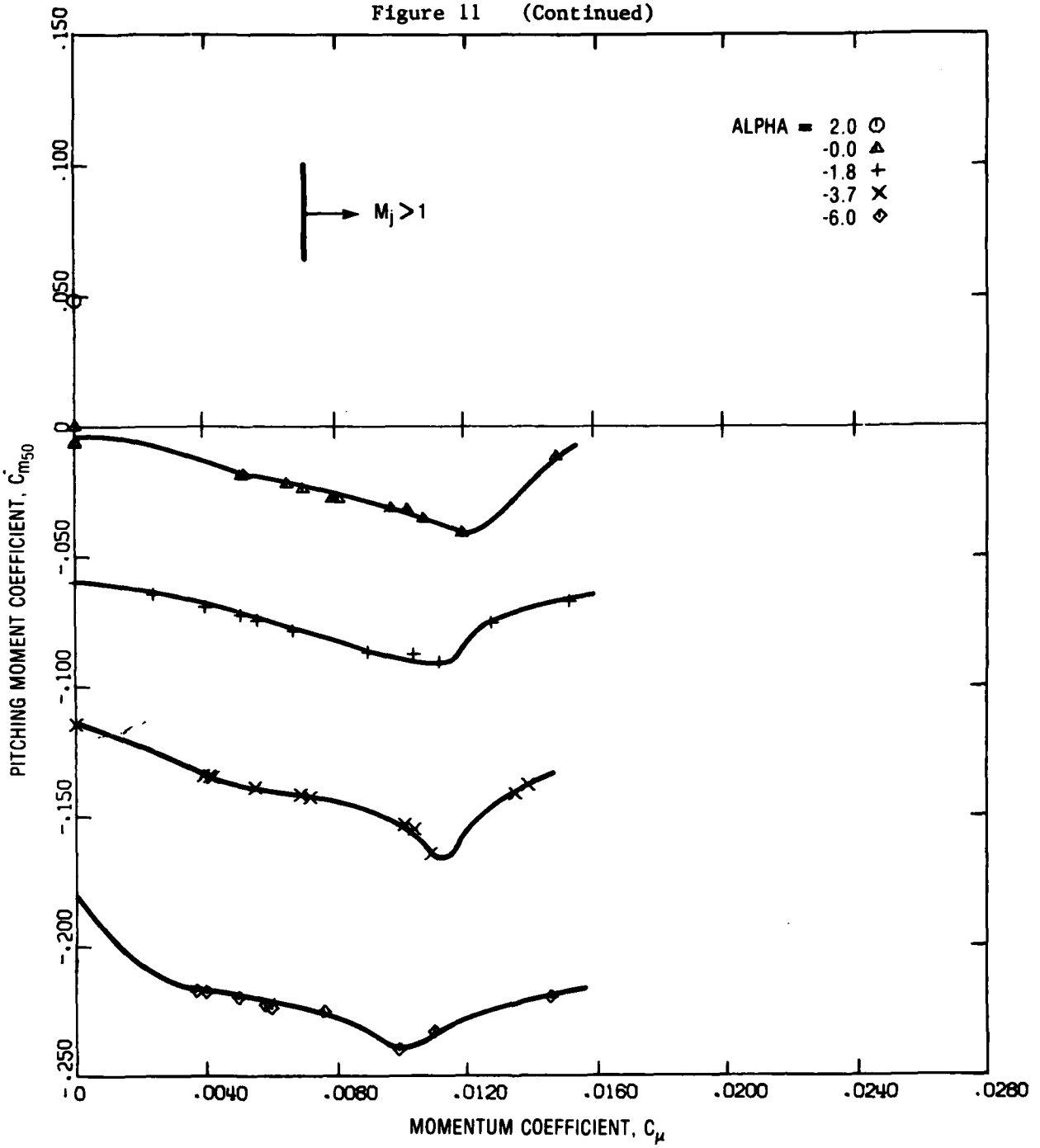

Figure 11e - Mach Number = 0.7

Figure 11 (Continued)

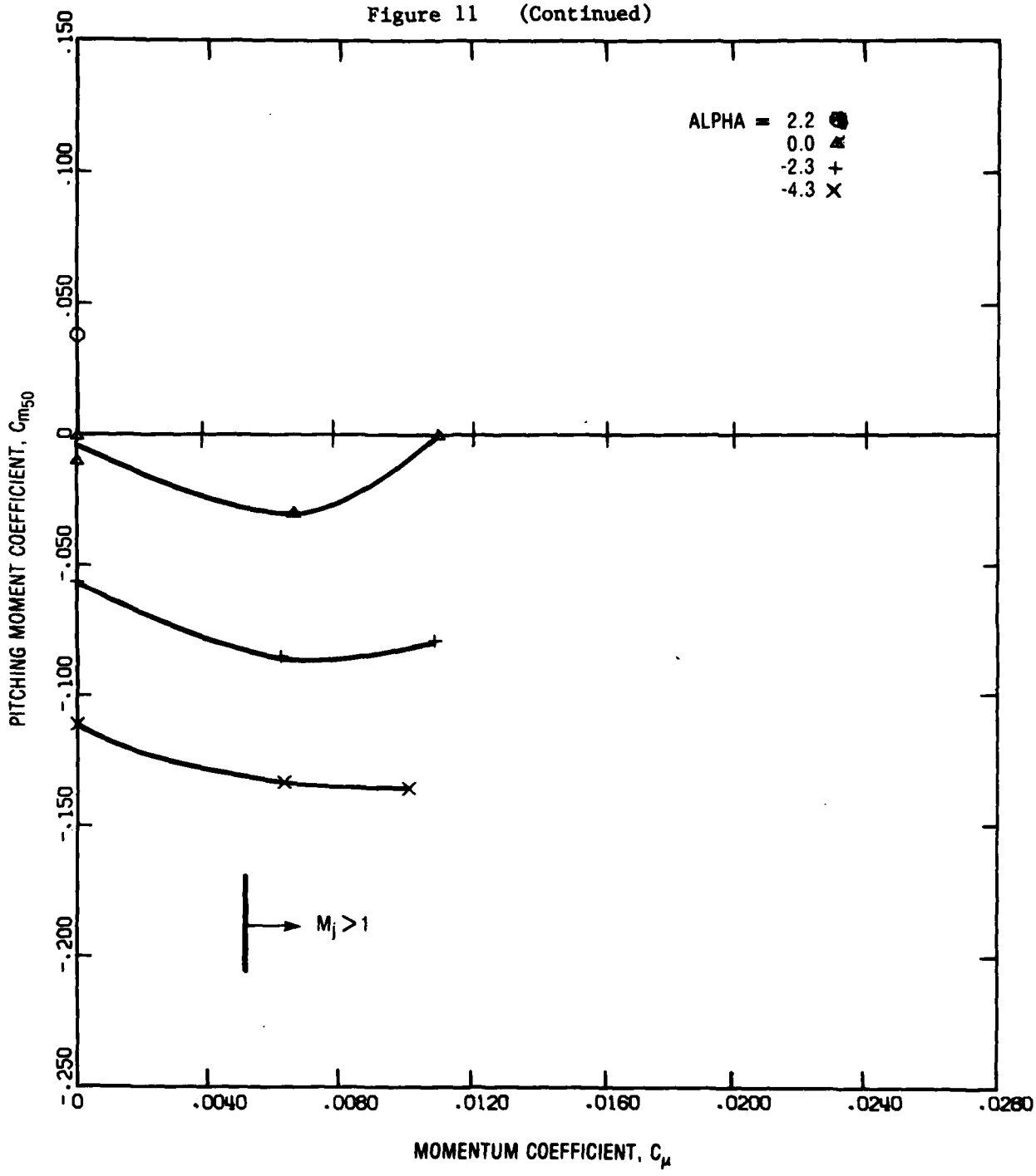

Figure 11f - Mach Number = 0.8

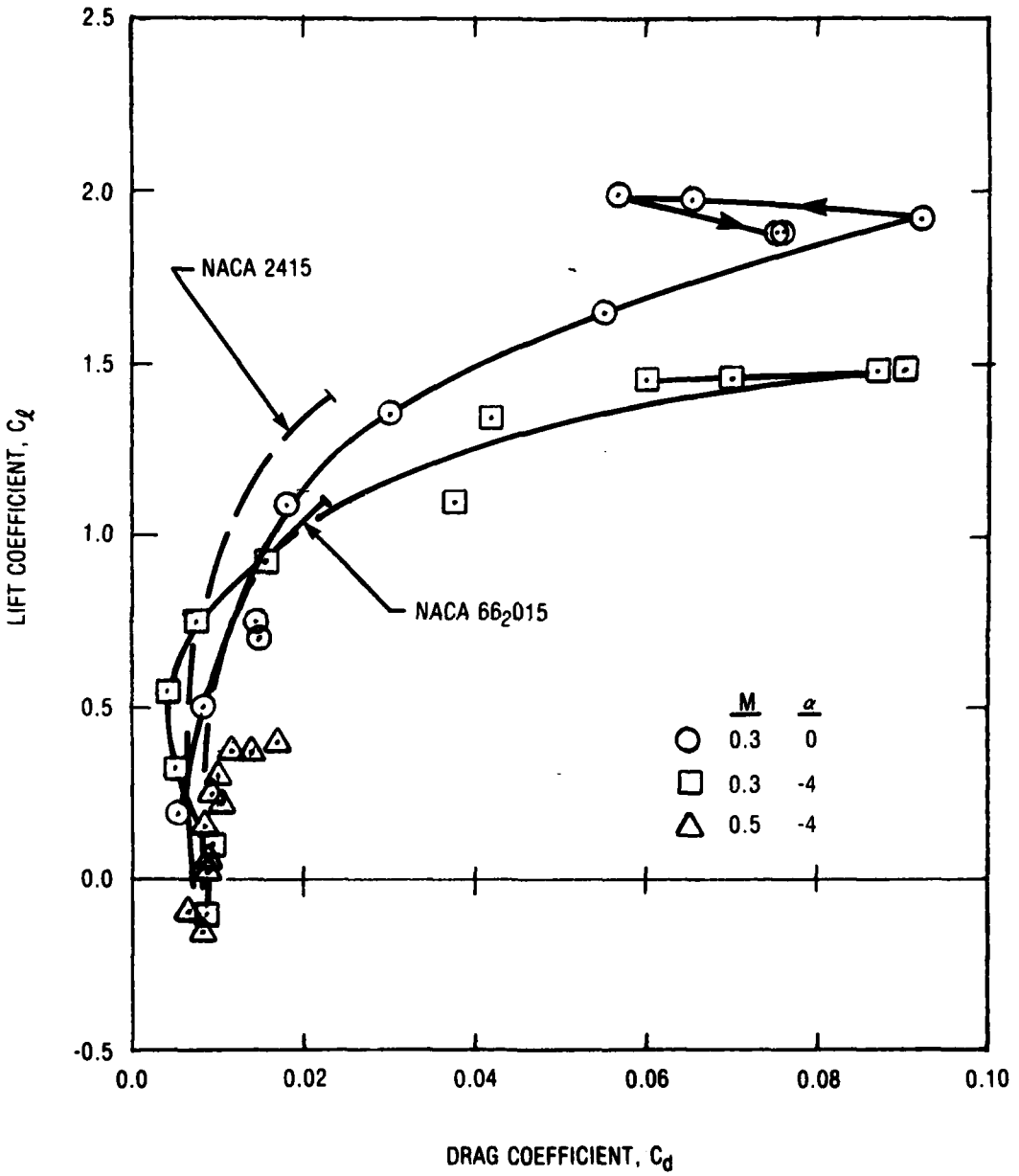

Figure 12 - Example Lift-Drag Polar for NCCR 1610-8054S Airfoil

Figure 13 - Lift Variation with Jet Momentum for Constant Angle of Attack

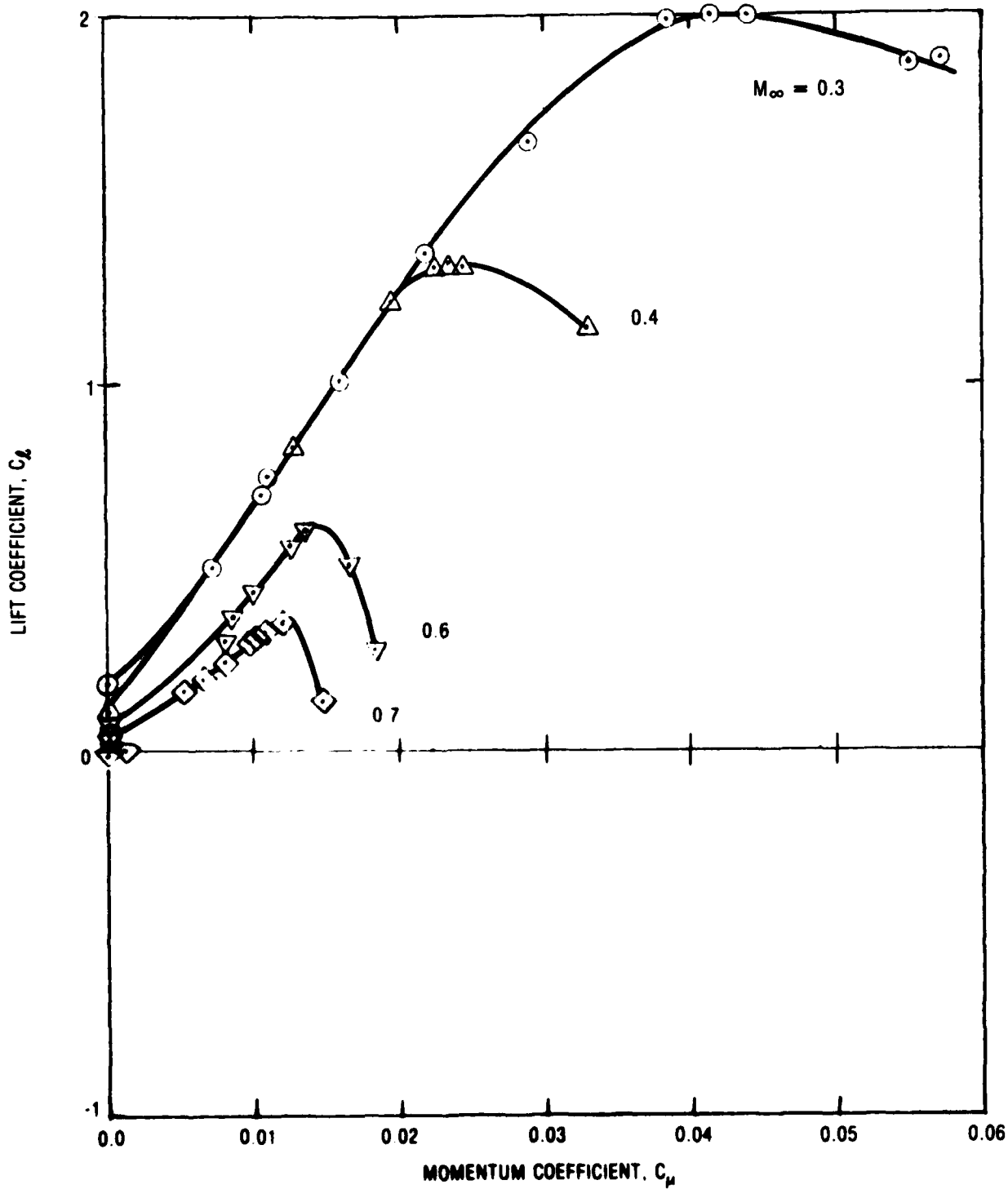

Figure 13a - Angle of Attack ≈ 0 Degrees

Figure 13 (Continued)

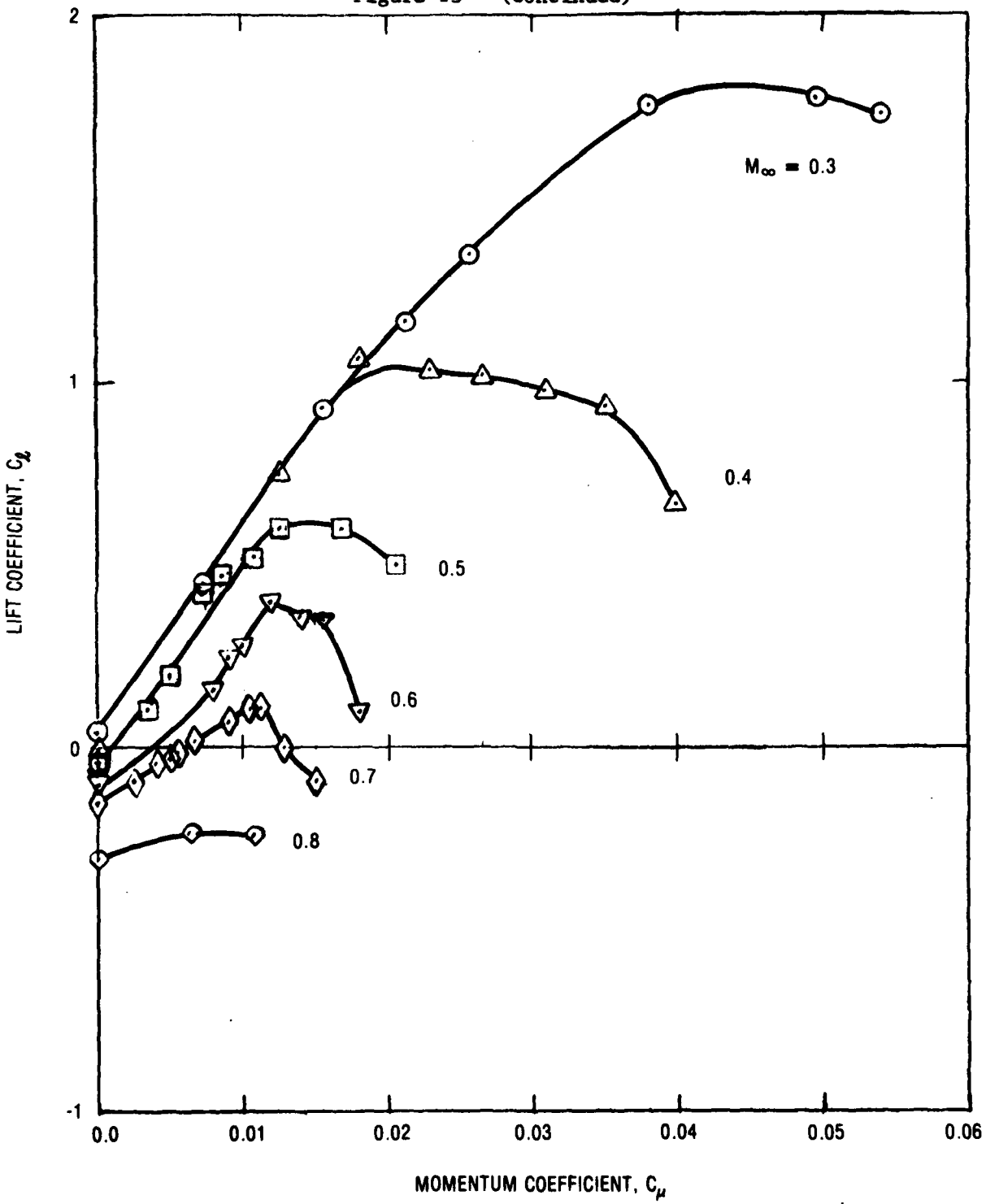

Figure 13b - Angle of Attack ≈ -2 Degrees

Figure 13 (Continued)

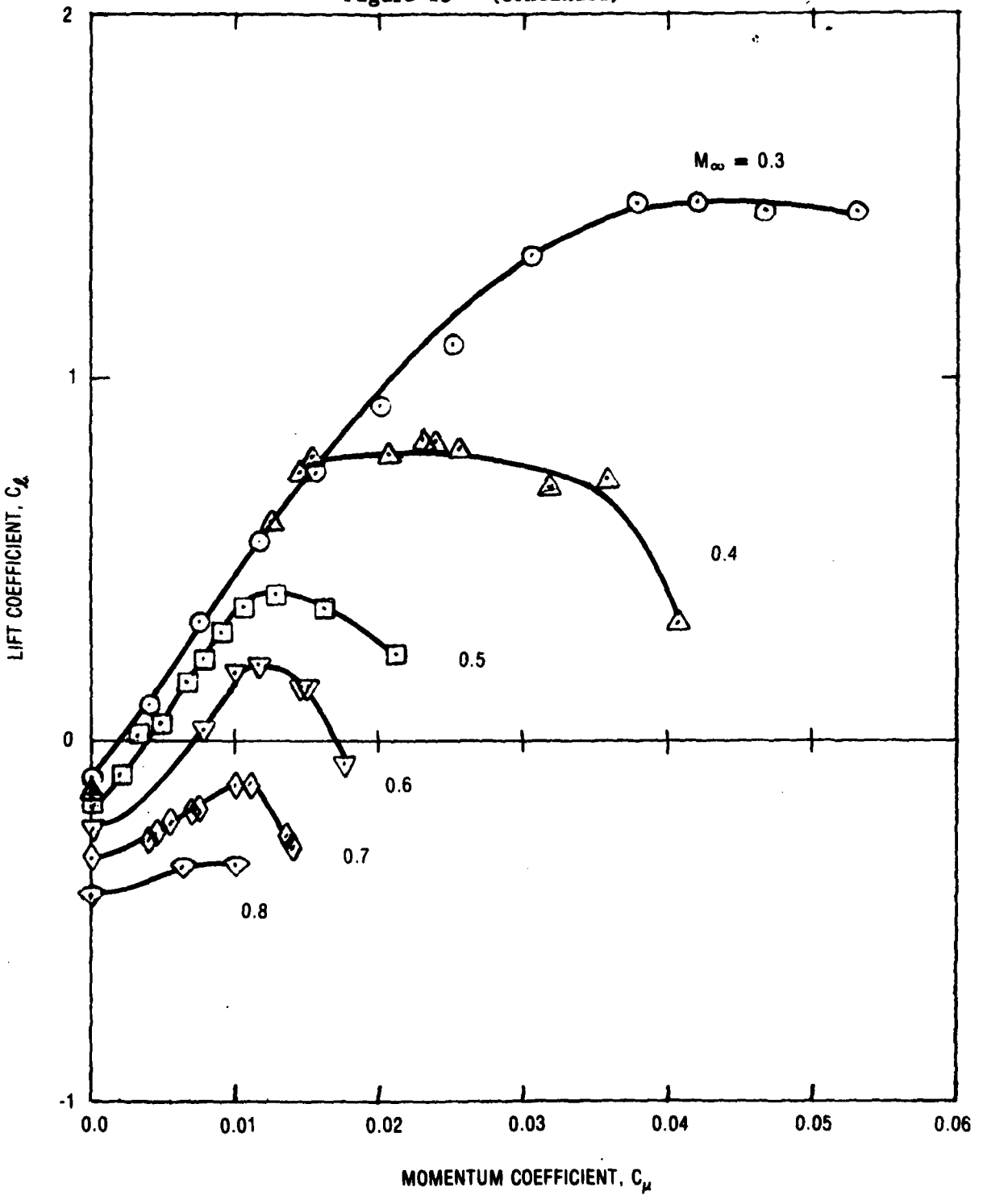

Figure 13c - Angle of Attack ≈ -4 Degrees

Figure 13 (Continued)

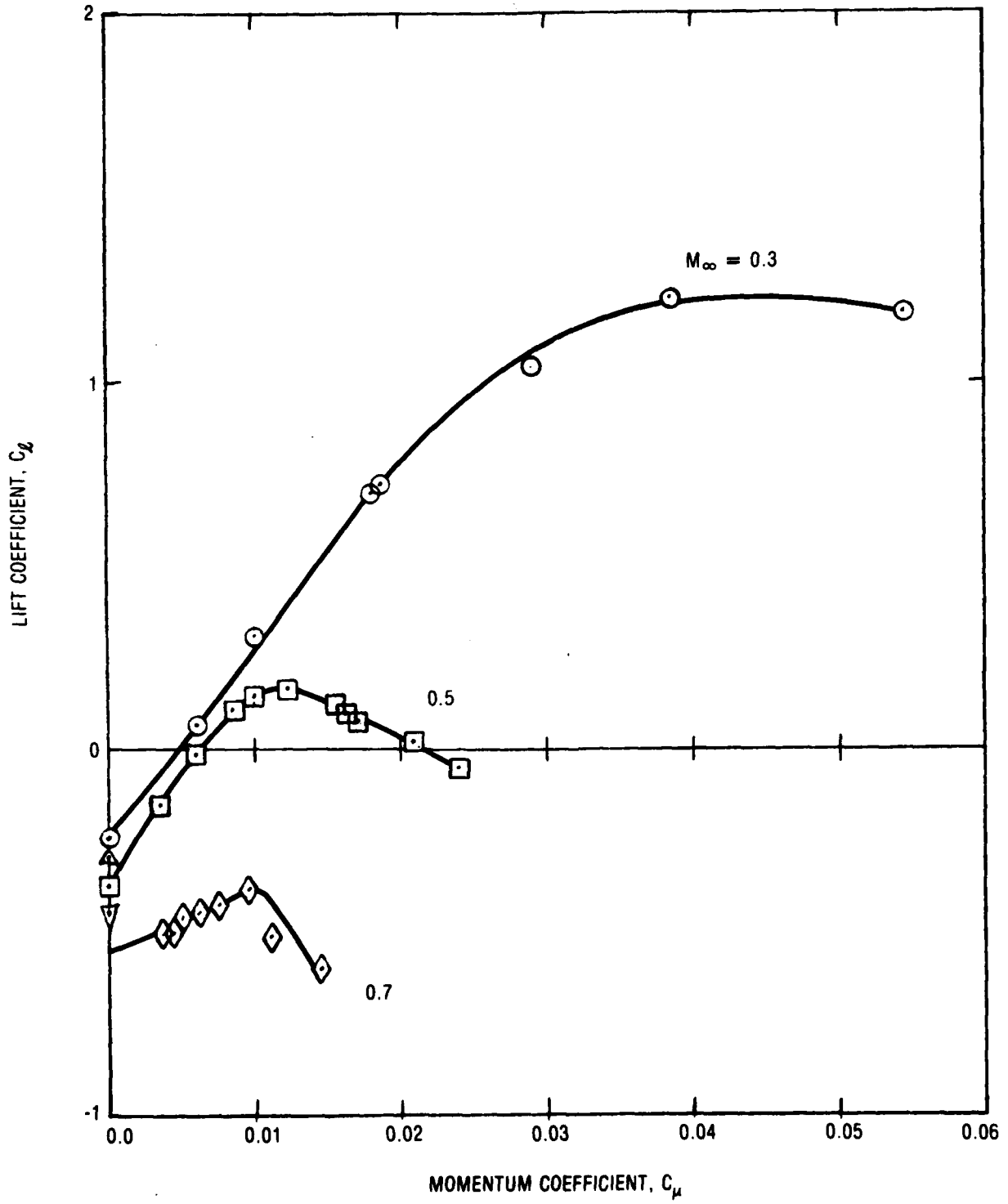

Figure 13d - Angle of Attack ≈ -6 Degrees

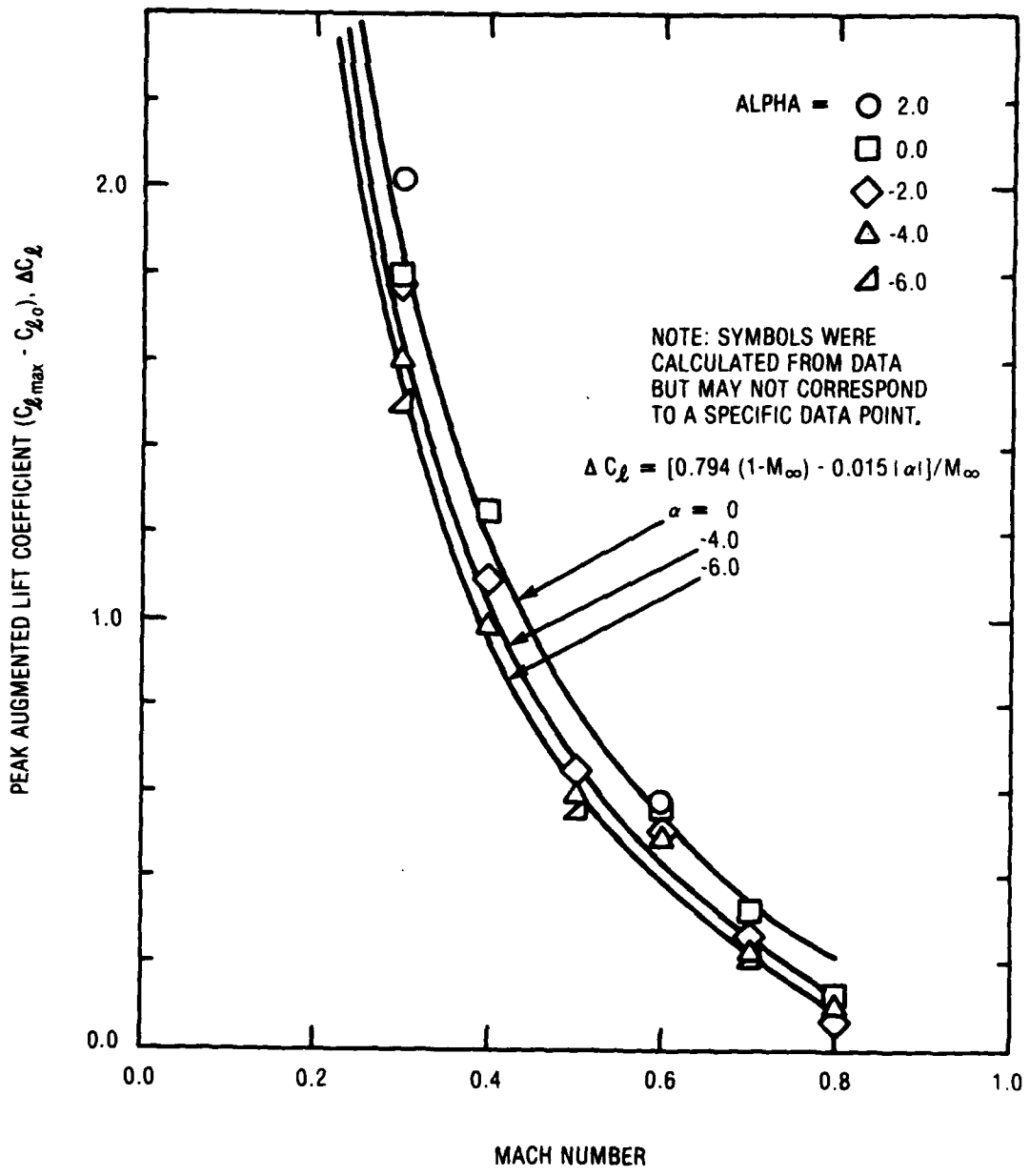

Figure 14 - Peak Augmented Lift Variation with Freestream Mach Number

Figure 15 - Pressure Distribution Variation with Jet Momentum Coefficient

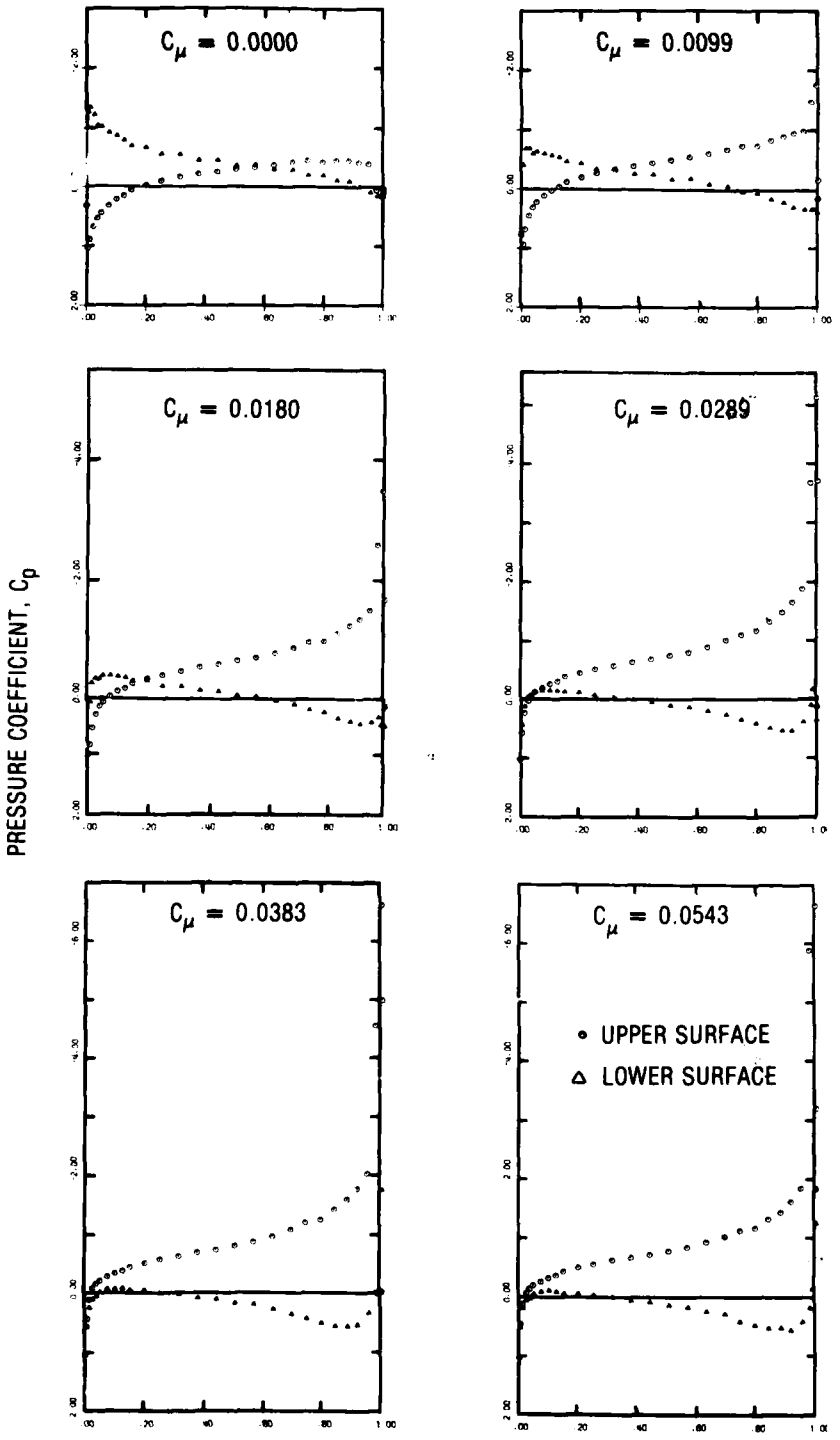

Figure 15a - M_∞ = 0.3, α = -6 Degrees

Figure 15 (Continued)

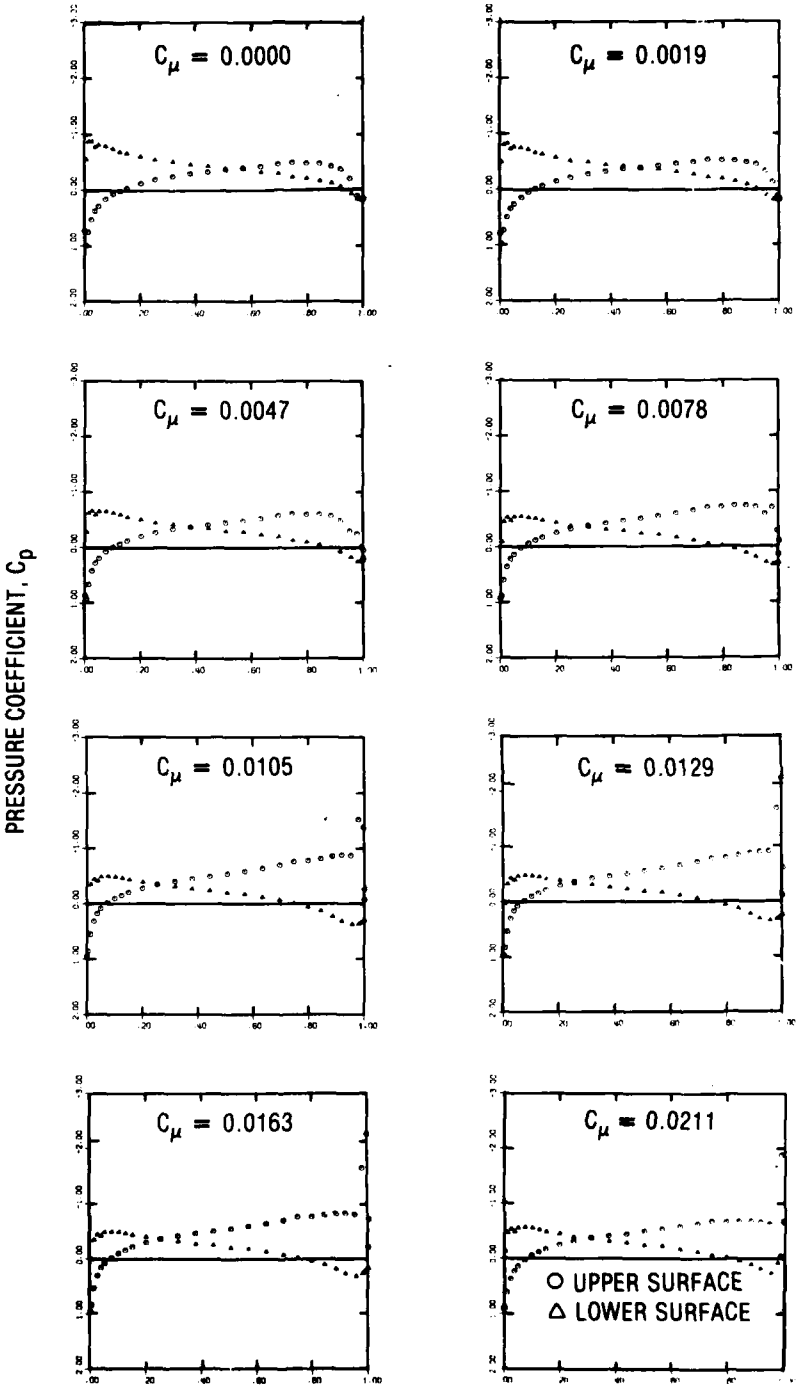

Figure 15b - M_∞ = 0.5, α = -4 Degrees

Figure 16 - Pressure Distribution Variation with Mach Number

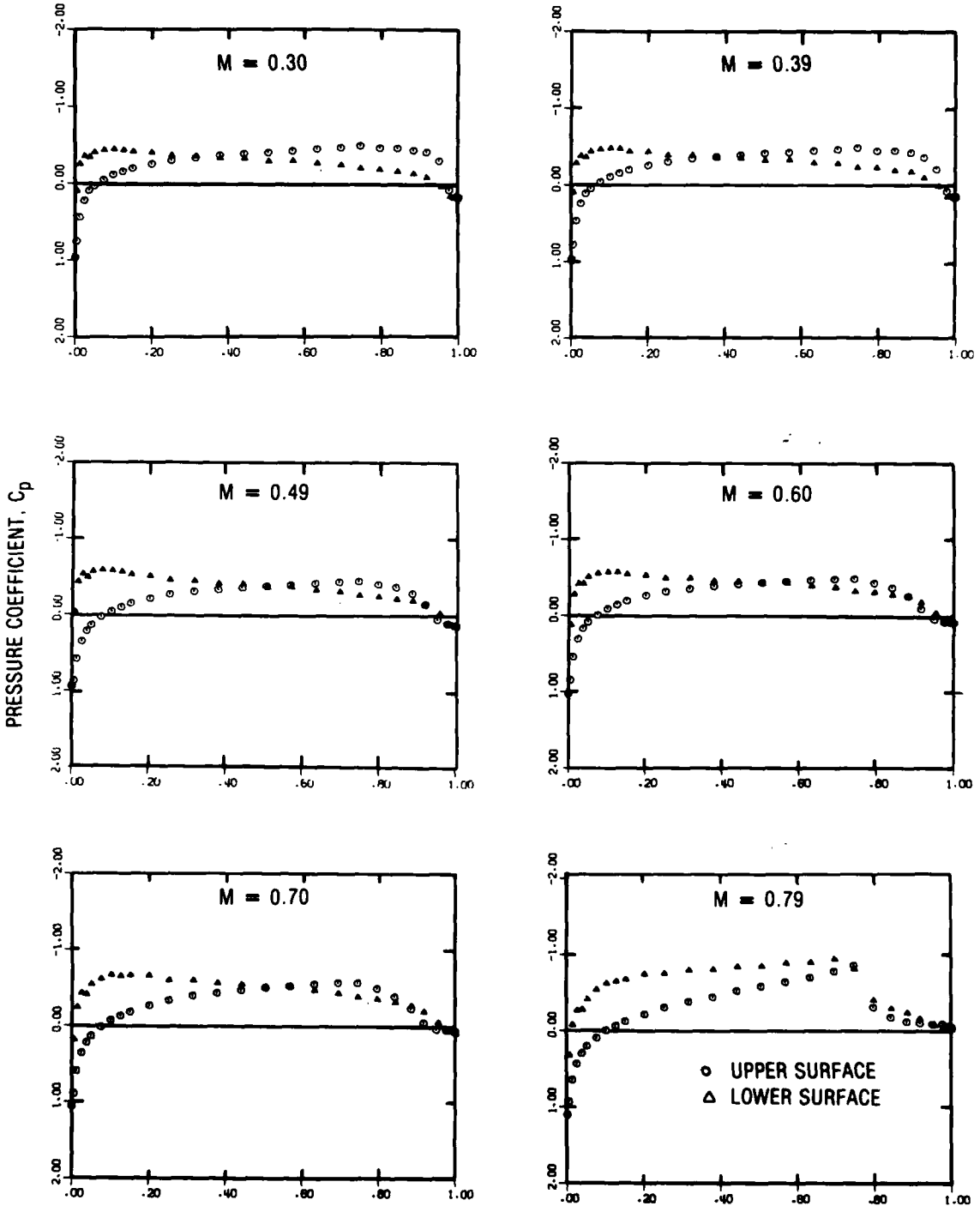

Figure 16a - $M_j = 0$, $\alpha = -2$ Degrees

Figure 16 (Continued)

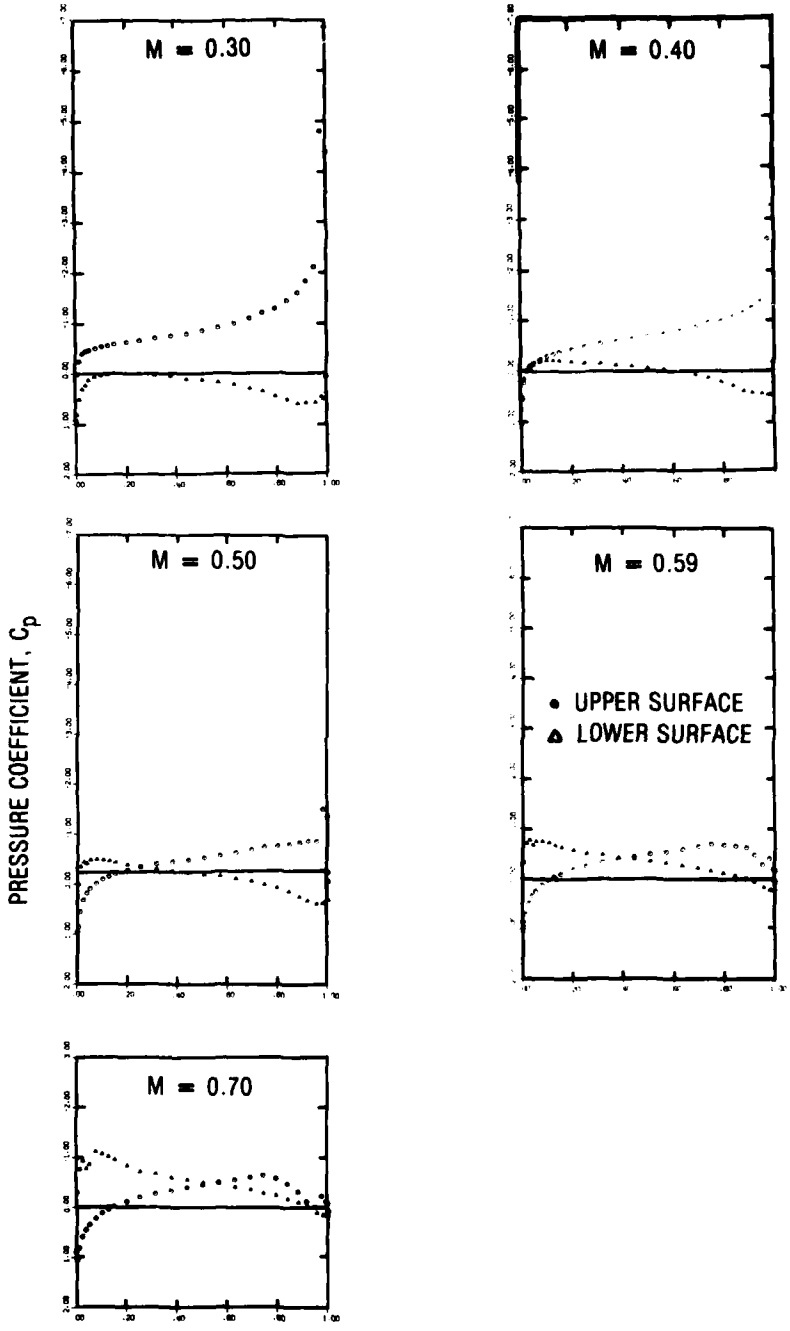

Figure 16b - $M_j \approx 0.89$, α = -4 Degrees

TABLE 1 - NONDIMENSIONAL AIRFOIL SURFACE COORDINATES AND PRESSURE TAP LOCATIONS

Chordwise Location	Thickness Location	Upper Surface								
		Spanwise Tap Locations (in.)								
x/c (%)	z/c (%)	-57	-48	-12	0[a]	+12	+24	+36	+48	+57
0.00	0.00				x					
0.49	1.03				x					
1.26	1.68				x					
2.48	2.39				x					
3.76	2.96				x					
5.04	3.43				x					
7.53	4.21				x					
10.08	4.86	x		x	x	x				x
12.59	5.47				x					
15.08	5.88				x					
20.10	6.72				x					
25.19	7.33				x					
31.50	8.03				x					
37.78	8.44				x					
44.10	8.78	x	x	x	x	x	x	x	x	x
50.40	8.92				x					
56.70	8.91				x					
63.10	8.72				x					
69.30	8.44				x					
74.40	8.06				x					
79.50	7.50	x	x	x	x	x	x	x	x	x
84.10	6.77				x					
88.30	6.05				x					
91.69	5.25				x					
95.00	4.23				x					
97.60	3.16	x	x	x	x	x	x	x	x	x
99.40	2.11				x					
100.06	0.49				x					
100.00	0.00	x	x	x	x	x	x	x	x	x

x - Pressure tap
a - Model mid-span location

TABLE 1 (CONTINUED)

Chordwise Location	Thickness Location	Lower Surface								
		Spanwise Tap Locations (in.)								
x/c (%)	z/c (%)	-57	-48	-12	0[a]	+12	+24	+36	+48	+57
0.00	0.00				x					
0.51	-1.01				x					
1.28	-1.63				x					
2.51	-2.31				x					
3.79	-2.85				x					
5.07	-3.29				x					
7.57	-4.01				x					
10.13	-4.57	x	x	x	x	x	x	x	x	x
12.64	-4.98				x					
15.14	-5.43				x					
20.00	-6.00				x					
25.20	-6.44				x					
31.60	-6.83				x					
37.89	-7.14				x					
44.20	-7.25	x	x	x	x	x	x	x	x	x
50.50	-7.24				x					
56.85	-7.12				x					
63.18	-6.83				x					
69.40	-6.50				x					
74.50	-6.13				x					
79.50	-5.61				x					
84.20	-5.31				x					
88.40	-4.61				x					
91.70	-4.02				x					
95.50	-3.25				x					
97.90	-2.39				x					
98.80	-1.77				x					
99.95	-0.16				x					
100.00	0.00	x	x	x	x	x	x	x	x	x

x - Pressure tap
a - Model mid-span location

DTNSRDC ISSUES THREE TYPES OF REPORTS

1. DTNSRDC REPORTS, A FORMAL SERIES, CONTAIN INFORMATION OF PERMANENT TECHNICAL VALUE. THEY CARRY A CONSECUTIVE NUMERICAL IDENTIFICATION REGARDLESS OF THEIR CLASSIFICATION OR THE ORIGINATING DEPARTMENT.

2. DEPARTMENTAL REPORTS, A SEMIFORMAL SERIES, CONTAIN INFORMATION OF A PRELIMINARY, TEMPORARY, OR PROPRIETARY NATURE OR OF LIMITED INTEREST OR SIGNIFICANCE. THEY CARRY A DEPARTMENTAL ALPHANUMERICAL IDENTIFICATION.

3. TECHNICAL MEMORANDA, AN INFORMAL SERIES, CONTAIN TECHNICAL DOCUMENTATION OF LIMITED USE AND INTEREST. THEY ARE PRIMARILY WORKING PAPERS INTENDED FOR INTERNAL USE. THEY CARRY AN IDENTIFYING NUMBER WHICH INDICATES THEIR TYPE AND THE NUMERICAL CODE OF THE ORIGINATING DEPARTMENT. ANY DISTRIBUTION OUTSIDE DTNSRDC MUST BE APPROVED BY THE HEAD OF THE ORIGINATING DEPARTMENT ON A CASE-BY-CASE BASIS.